國立臺灣大學工學院化學工程學系

碩士論文

Department of Chemical Engineering

College of Engineering

National Taiwan University

Master Thesis

合成類沸石咪唑骨架材料(ZIF-8)衍生之摻氮多孔碳材並應用於糠醛至馬來酸之轉化

Synthesis of ZIF-8-Derived Nitrogen-Doped Nanoporous Carbon for Furfural-to-Maleic Acid Conversion

巫婧柔

Jing Rou Boo

指導教授：吳嘉文 博士

Advisor: Chia-Wen Wu, Ph.D.

中華民國 108 年 6 月

June, 2019

doi:10.6342/NTU201901225

致謝

此研究能順利完成，首先感謝指導教授，吳嘉文老師，除了在實驗上給予指導，更提供了豐富的資源，讓我們可以盡情的做研究。很榮幸可以加入這個大家庭，并有機會參加各種研討會，增光見聞的同時也見識到自己的渺小與不足。

在實驗室學到的，除了獨立思考的邏輯，還有人與人的相處。非常感謝Sagar、Chi 、俊毅、正彥、韓柏，在我剛進實驗室，毫無方向感到迷茫時給予指點及建議。尤其是俊毅，在我碩一期間給予很大的幫助，無論是實驗技巧或專業知識，甚至生活上的困難等等。再來要感謝我的戰友宏霖、妤欣及襄伶。特別是在碩一最無助彷徨，同時面對課業與研究進度壓力時，感謝有你們的陪伴，并且在課業上給予了我很多的協助。特別感謝共患難的宏霖，雖然你有時候雷雷的，但彼此的互相鼓勵都成爲當初堅持下去的動力。也感謝智偉，在我失落的時候給予的鼓勵與支持。當然還要感謝學長姐祐德、任軒、希彥、瀅惠及偉琪對實驗室的付出。另外感謝學弟妹，嘉軒、晏慈、瑋呈、怡婷及祐陞幫忙分擔實驗室的雜事，也讓實驗室的氣氛歡樂融洽。另外，特別感謝總是盡心盡力幫大家處理行政事務的欣昱。

感謝家人，尤其是從小照顧我的阿公阿嬤，來臺灣的這些年很少回去陪伴你們，這期間靠著自己的努力和運氣，如今我也讀到碩士畢業了，應該也足以成爲你們的驕傲吧！

感謝自己，在 6 年前有勇氣獨自一人離鄉背井，來到臺灣展開一段嶄新的旅程，且一直都勇敢的抬頭挺胸面對一切。

在實驗室的這兩年，經歷了許多的過客，感覺就像一班長途列車，搭乘過的有來自日本、韓國、德國、印度、泰國、越南、菲律賓、馬來西亞、澳門等不同國家的人。相處的時間有長有短，而在這一個停靠站，輪到我們要下車了。感謝命運和緣分讓我們相遇，這不是終點而是啓程，期待未來更好的自己與大家再相逢！

doi:10.6342/NTU201901225

Abstract

Maleic acid (MA) and maleic anhydride are important C_4 chemical intermediates to produce high value-added chemicals. In industry, maleic anhydride is commercially produced through petrochemical route by the oxidation of the exhaustible and non-renewable feedstocks, n-butane and benzene. On the other hand, the renewable resource, furfural derived from lignocellulosic biomass, has been recognized as a potential bio-based platform chemical to produce MA through catalytic oxidation. Until now, the conversion of furfural to MA has been mainly catalyzed by an acidic catalyst, which exhibited several drawbacks. Here, we report the first acid-free system for furfural to MA conversion, by using the nitrogen-doped nanoporous carbon material (NC) derived from zeolitic imidazolate frameworks (ZIF-8). The synthesized ZIF-8 was undergoing direct carbonization at different temperatures in order to investigate the effect of carbonization temperature on nitrogen configuration in the resulted carbon materials. The effect of reaction parameters, including H_2O_2 concentration, solvent, reaction temperature and time were systematically studied. A MA yield as high as 61 % was achieved over NC-900 catalyst at 80 °C in 5 hours, assisted by 35 wt% H_2O_2. The kinetics study indicates that the mechanism was via the oxidative ring-opening reaction and formation 5-hydroxy-furan-2(5H)-one as the main intermediate, following by Baeyer-Villiger oxidation, rearrangement steps, and hydrolysis to form MA.

Keywords: maleic acid, furfural, oxidation, nitrogen-doped carbon, zeolitic imidazolate frameworks.

doi:10.6342/NTU201901225

摘要

馬來酸 (maleic acid; MA) 和馬來酸酐 (maleic anhydride) 為重要的四碳化合物，常被用於生產高附加值的化學品。然而在傳統工業中，馬來酸酐的生產是透過石油化學途徑，藉由氧化正丁烷和苯等可耗盡且不可再生的原料製備而成。反之，自生物質轉換所得之可再生資源，糠醛，也可經由氧化催化反應製備馬來酸。過去有關於糠醛製備馬來酸的轉化，大多以酸性催化爲主並存在許多的缺點。因此，本研究使用衍生自 ZIF-8 的摻氮多孔碳材 (NC)，首次在非酸性的環境中，將糠醛氧化轉化成馬來酸。ZIF-8 是一種典型的類沸石咪唑骨架材料 (ZIF)，可作爲自體模板，進一步鍛燒加以碳化得到摻氮之多孔碳材。本研究將 ZIF-8 於不同溫度下進行碳化，以探討碳化溫度對碳材之氮原子組態的影響。我們也研究了各種反應參數，包含溶劑，雙氧水濃度，反應溫度和時間對 MA 產率的影響。透過 NC-900 催化劑，雙氧水 (35 wt%) 作為氧化劑，在 80 °C 下，我們可在 5 小時內達成最高 61% 之馬來酸產率。我們推測此反應之路徑是透過氧化開環，形成 5-羥基-2(5H)-呋喃酮 (5-hydroxy-furan-2(5H)-one) 作為主要中間產物，隨後進行 Baeyer-Villiger 氧化，重排步驟和水解，進而得到馬來酸 。

關鍵字: 馬來酸，糠醛，氧化，摻氮碳材，類沸石咪唑骨架

doi:10.6342/NTU201901225

Table of Content

doi:10.6342/NTU201901225

doi:10.6342/NTU201901225

List of Figures

doi:10.6342/NTU201901225

doi:10.6342/NTU201901225

List of Tables

doi:10.6342/NTU201901225

1. Introduction

1.1. Maleic anhydride and maleic acid

Maleic anhydride (MAN) and maleic acid (MA), are important C_4 chemical intermediates with many applications in the chemical industry. The production of one of them implies the availability of the other because MA and MAN can be interconverted into each other by hydration or dehydration steps. They are important raw materials for the production of unsaturated polyester resins, vinyl copolymers, lubricant additives, plastics, γ-butyrolactone (GBL), 1,4-butanediol (1,4-BDO), tetrahydrofuran (THF) and N-methylpyrrolidone (NMP)[1-3]. Succinic acid and fumaric acid, which both having multiple additional applications, are also synthesized from MA and/or MAN. According to the research report issued by Transparency Market Research (TMR), the global maleic anhydride market was valued at US$ 4.11 billion in 2012, and it is likely to reach a value of US$ 5.96 billion, rising at a 6.4% CAGR from 2012 to 2018. At the same time, the volume of the maleic anhydride market in worldwide is expected to reach 2,752.4 tons by the end of 2018.[4] Figure 1.1 shown the increasing trend of global maleic anhydride market from 2011 to 2018.

In industry, maleic anhydride is commercially produced through petrochemical route, which carried out by the catalytic oxidation of petroleum-based chemicals such as n-butane and benzene, which is exhaustible and non-renewable feedstock.[5,6] Instability in the prices of non-renewable resources coupled with environmental issues were expected to be the major restraining factor for the production of petroleum based maleic anhydride. Therefore, alternative routes to produce maleic acid and maleic anhydride based on renewable resources has been explored by different research groups. Among various renewable platform compounds, furfural was found to be potential to derive the C_4 di-acids or anhydride acids.

doi:10.6342/NTU201901225

Figure 1.1 Global maleic anhydride market from 2010 to 2018

1.2. Furfural

Due to the increasing consumption of energy and depletion of petroleum feedstocks, various forms of renewable energy resources have been explored to develop sustainable processes. Biomass, an environmental-friendly and renewable carbon source, is considered to be an ideal substitute for traditional fossil fuels.[7,8]

In recent years, various catalytic conversion strategies have been developed for the conversion of biomass to bio-based platform compounds, which can be further converted to a wide range of target products.[9-12] Among various renewable platform compounds, furfural is one of the most important building blocks for bio-refinery. It is a commercially available chemical product derived from lignocellulosic agricultural residues, such as wood waste, corn cobs, and sugar cane residues, at an annual production rate of ca. 300 kton.[13,14] Through hydrolysis and dehydration of xylan contained in hemicellulose, furfural can be produced.[15] Moreover, furfural has been selected as one of the top 10 chemical from carbohydrates which can be further converted to an assortment of valuable material with more than 1600 commercial products.[16]

doi:10.6342/NTU201901225

In fact, the production of biofuels from furfural has received extensive attention over the past decades. A typical example is the selective hydrogenolysis of furfural into potential fuel components such as 2-methylfuran (2-MF) and 2-methyltetrahydrofuran (2-MTHF).[17,18] In addition, furfural can be also converted to a variety of valuable C_4 and C_5 chemicals.[19] Most of the C_5 chemicals are produced through selective hydrogenation or hydrogenolysis, while the C_4 chemicals are mainly synthesized through selective oxidation as the first step. Therefore, the investigation of the catalyst and reaction condition converting furfural into desired product in high selectivity is important.

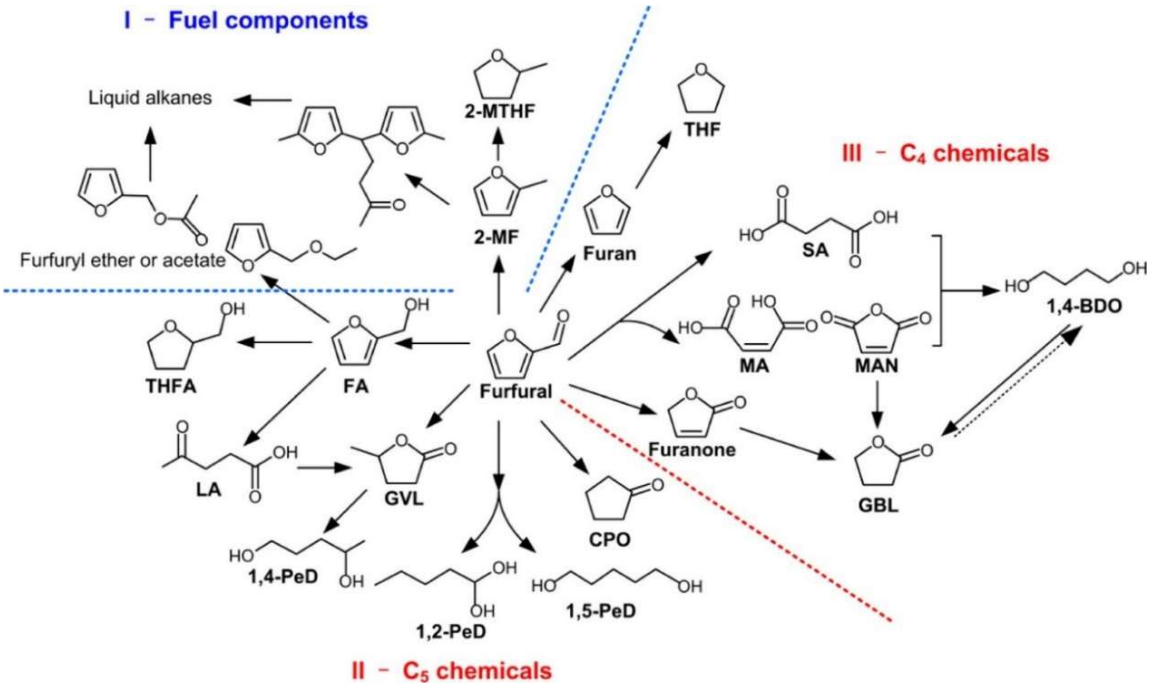

Figure 1.2 Catalytic conversion of furfural to chemicals and fuel components[19]

doi:10.6342/NTU201901225

1.3. The metal-free catalyst

Catalysis is one of the most important field in chemical reaction which apply to the industrial chemical production process. In the past several decades, heterogeneous catalysis is highly attractive owing to their advantages of recyclability and synergetic effect. Metals and metal oxides are widely used as catalysts for materials production, clean energy generation and storage, and many other important industrial processes. However, metal-based catalysts suffer from high cost, low selectivity, poor durability, susceptibility to gas poisoning and have a detrimental environmental impact.

In recent years, the metal-free materials appear as a new class of heterogeneous catalyst, in order to meet the requirement of green and sustainable chemistry.[20-22] Among various kind of metal-free catalysts, carbon materials are always the most attractive candidates due to their large surface area, excellent chemical and mechanical stability, tunable porosity, and high diversity.[23,24] As listed in Table 1.1, several carbon-based metal-free catalysts have been demonstrated to be effective for several catalytic processes.

doi:10.6342/NTU201901225

Table 1.1 Summary of several carbon-based metal-free catalysts

Materials	Catalyst preparation	Catalytic application	Catalytic efficiency	Ref.
N-doped VA-CNTs	Pyrolysis of iron phthalocyanine in NH_3	ORR	> Pt/C	25
N-doped graphene	CVD of CH_4 and NH_3	ORR	> Pt/C	26
B-doped CNTs	CVD of benzene–TPB–ferrocene mixture	ORR	< Pt/C	27
N-doped graphite nanomaterials	Melamine formaldehyde	OER	> Pt/C	28
Carbon nanofibers	Pyrolysis of electrospun nanofiber	CO_2 reduction	Overpotential (0.17V)	29

doi:10.6342/NTU201901225

1.3.1. Nitrogen-doped nanoporous carbon

Doped carbons are carbon-based materials containing significant amounts of other elements besides carbon, hydrogen and oxygen, such as nitrogen, boron or phosphorus. The most common dopant element is nitrogen, since it has a similar size to carbon and one electron more than carbon in the external shell. In the recent advances of carbon-based functional materials, the nitrogen-doped carbon materials have shown great potential in several fields.[30] The methods for the preparation of nitrogen-doped carbon materials has been classified into two groups, the post-treatment of carbons and *in situ* synthesis method.[31,32]

Post-treatment method refers to direct thermal treatment of carbon with nitrogen-containing precursors. The primary carbons include different materials, such as activated carbon, carbon nanotubes (CNTs), graphene oxide (GO) and reduced graphene oxide (RGO), while nitrogen-containing precursors including urea, melamine, ammonia, cyanamide, and polyaniline.

***In situ* synthesis method** is relatively simple and effective compared with post-synthesis method, because various kind of precursors are readily available and it enables a homogenous nitrogen-doping throughout the bulk material. Many strategies have been developed to synthesis NCs through *in situ* method, for example, chemical vapor deposition (CVD) and direct pyrolysis of nitrogen-containing complexes. CVD is a method used widely in the preparation of carbon nanomaterials, such as graphene, carbon fibers and carbon nanotube. On the other hand, direct pyrolysis of nitrogen-containing complexes to become NCs is a very straightforward yet efficient way to prepare porous carbon materials. Some typical examples of nitrogen-containing complexes are metal-organic framework (MOFs), biomass and ionic liquid.

doi:10.6342/NTU201901225

Here, we would like to mainly discuss the direct pyrolysis of nitrogen-containing precursor, metal-organic framework (MOF) into nitrogen-containing porous carbon material.

1.3.2. Metal-organic framework (MOFs)

Metal-organic frameworks (MOFs), also known as porous coordination polymers (PCPs), have emerged as a new class of crystalline porous materials, which have been utilized as alternative precursors for synthesizing nanostructured materials with controllable particle size and morphology.[33] MOFs are constructed by the coordination of inorganic metals ions (secondary building units, SBUs) with organic linkers, as depicted in Figure 1.3. The variety of metal ions, organic linkers and structural motifs provide an infinite number of possible combinations through control of the architecture and functionalization of the pores.

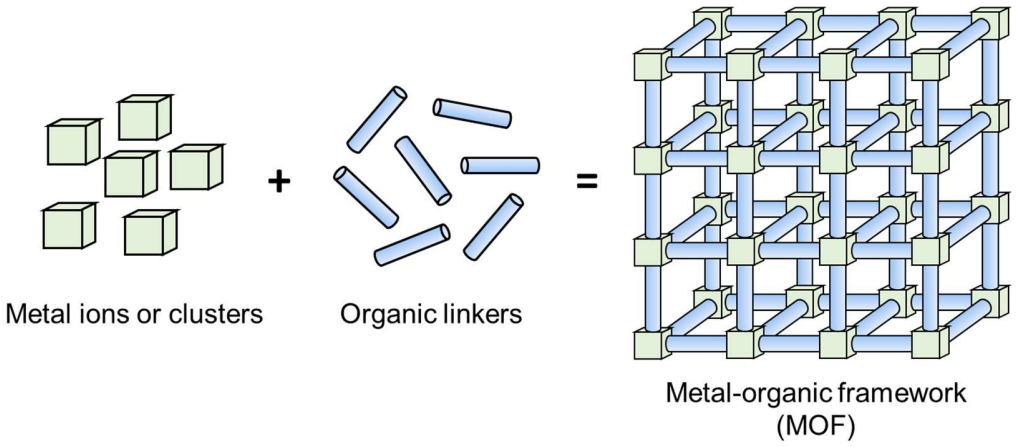

Figure 1.3 Schematic diagram of MOF building blocks

doi:10.6342/NTU201901225

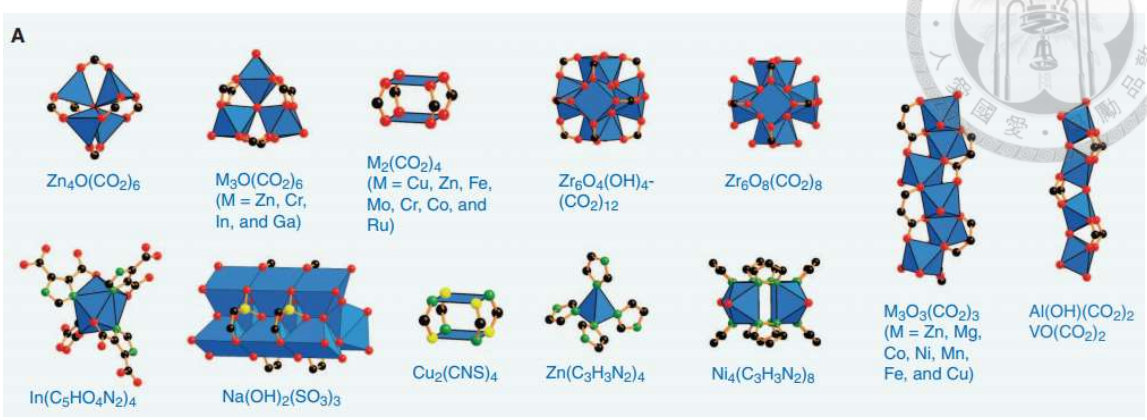

Figure 1.4 Building block of MOFs (A) Inorganic secondary building units[33]

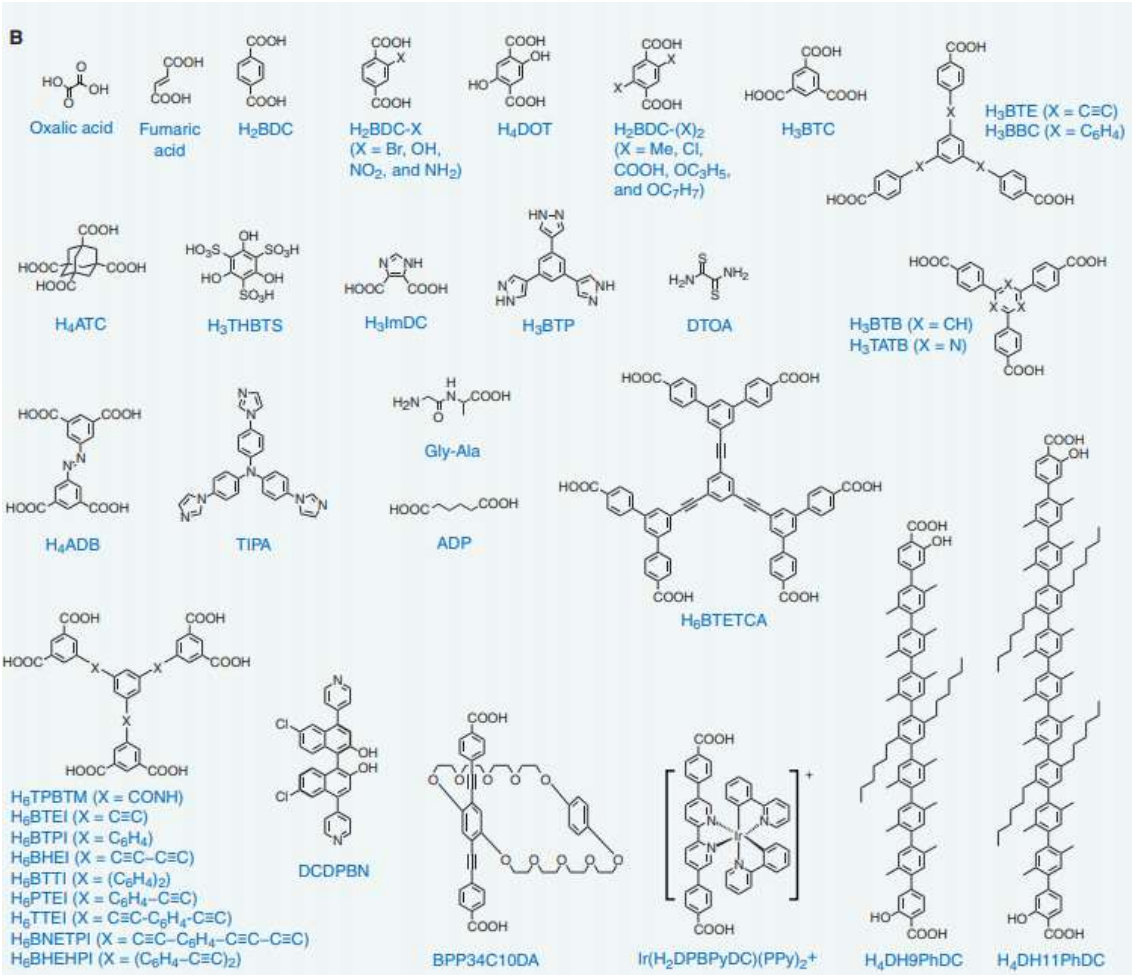

Figure 1.5 Building block of MOFs (B) organic linkers of MOFs[33]

doi:10.6342/NTU201901225

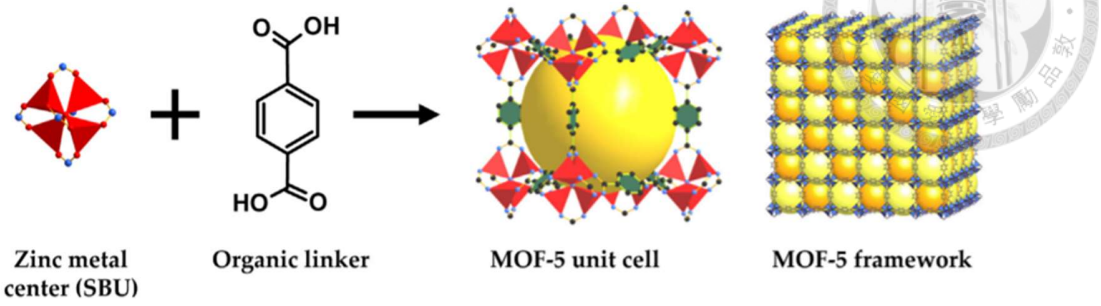

Figure 1.6 Illustration of MOFs construction[34]

The specific surface area of such MOFs typically ranges from 1000 to 10,000 m^2 /g, exceeding those traditional porous materials such as zeolites and carbons.[33] Due to the diverse structure, versatile functionalities, tunable properties, and regular crystalline structures, MOFs have attracted extensive research interest and having applications in different fields, such as gas storage[35], separation[36], drug delivery[37], sensing[38] and catalysis[39]. More than 20000 different types of MOFs have been reported and studied within the past decade,[33] and the utilization of MOFs in catalysis have been paid attention in recent years (e.g. ZIF-8, HKUST-1, MIL-53, UiO-66, and PCN-222).

In order to further improve the properties and introduce new functionalities to MOFs for catalysis, different attempts have been made. Other than the direct use of the active sites in the framework of MOFs, the MOF-derived catalysts also synthesized through the functionalization of MOFs with other ligands, and the thermal treatment of MOFs to become porous carbon or metal oxide.[40] Due to highly ordered and uniform porous structure, the MOF-derived materials are able to develop porous carbons/metals/metal oxides with uniform pores at different scales. And due to their permanent nanoscale cavities and open channels, which are similar to mesoporous silica and zeolites, MOFs exhibit a strong potential for use as templates and reactive precursors for synthesizing nanoporous carbon materials.

doi:10.6342/NTU201901225

1.3.3. MOFs-derived nitrogen-doped nanoporous carbon

The *in situ* pyrolysis of metal-organic frameworks (MOFs) had demonstrated as a fascinating route to prepare the carbon-based material. The first reported MOFs as a template to generate porous carbons was demonstrated by Liu's group[41]. Until now, several representative MOFs were used to create nanoporous carbons, such as MOF-5, Al-PCP and ZIF-8[42 30], as shown in Figure 1.7. During thermal carbonization in an inert atmosphere, the formation of porous carbon networks and the decomposition of MOFs occur simultaneously. Therefore, MOFs function as both a sacrificial template and a secondary carbon precursor. The heating rate, carbonization time and MOF ligands playing an important role in the resulting carbon materials.[43] MOFs-derived materials exhibited the unique advantage of high specific surface area, porosity, and abundant active sites from mother MOFs. By altering ligands and metal ions, the texture properties of MOFs-derived materials could be customized for different applications.

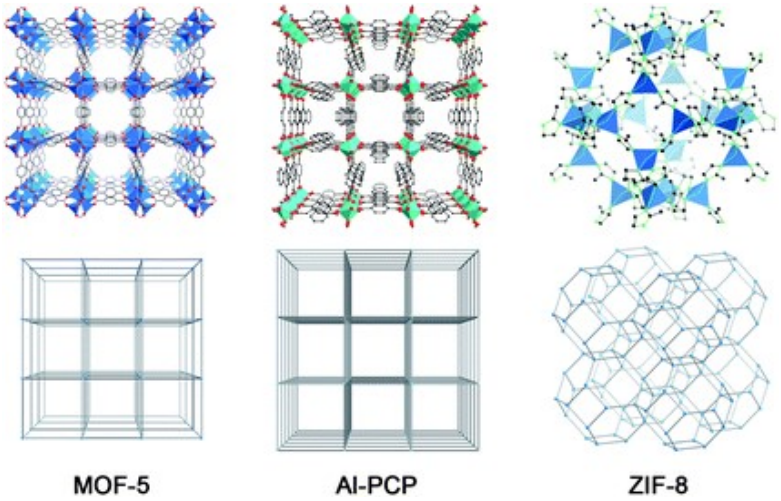

Figure 1.7 Typcial example of MOFs to derive nanoporous carbons[30]

doi:10.6342/NTU201901225

1.3.4. ZIFs-derived nitrogen-doped nanoporous carbon

Zeolitic imidazolate frameworks (ZIFs) are a class of metal-organic frameworks (MOFs) that having topological isomorphism with zeolites.[44-46] Typically, ZIFs composed of tetrahedrally-coordinated transition metal ions (e.g. Fe, Co, Cu, Zn) connected by the imidazolate linkers. Various type of imidazolate linkers can be interconnected with the metal ions to form different structures of ZIFs as depicted in Figure 1.9. The metal-imidazole-metal angle in ZIFs are similar to the 145° Si-O-Si angle in zeolites, thus ZIFs possess zeolite-like topologies. The element arrangement of ZIFs are illustrated in Figure 1.8.

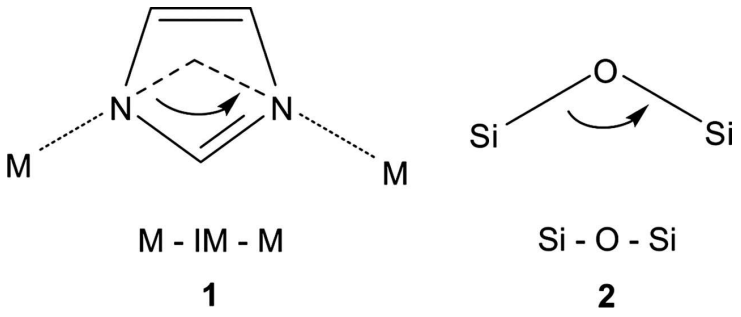

Figure 1.8 The bridging angles in (1) metal MeIM and (2) zeolites[46]

doi:10.6342/NTU201901225

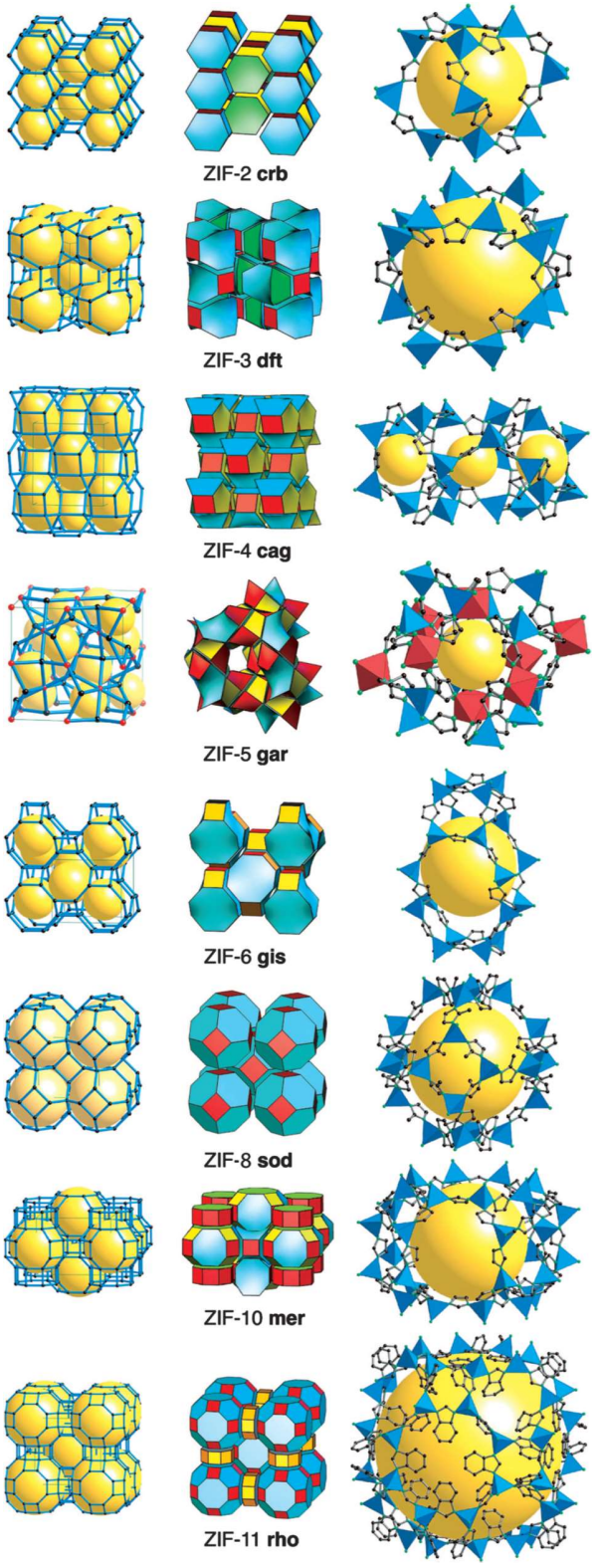

Figure 1.9 Single crystal x-ray structures of various ZIFs[46]

doi:10.6342/NTU201901225

A typical representative example of zeolitic imidazolate frameworks (ZIFs) is the zeolitic imidazolate framework-8 (ZIF-8), which exhibits a sod topology comprised of 1.16 nm cages connected through six-membered windows, 0.34 nm in size and with high specific surface area.[47,48] ZIF-8 is currently the most widely investigated ZIF material for a range of applications, and it has been commercialized (Basolites Z1200, BASF). ZIF-8 framework consists of the Zn^{2+} transition metal ion and nitrogen-containing 2-methylimidazolate linkers (34 wt% N), which form three-dimensional frameworks resembling the zeolite topology. ZIF-8 can be prepared in high purity through different synthesis routes. Synthesis under an environmentally friendly manner under facile conditions is highly desirable and therefore particular emphasis has been placed upon size-controlled ZIF-8 synthesis.

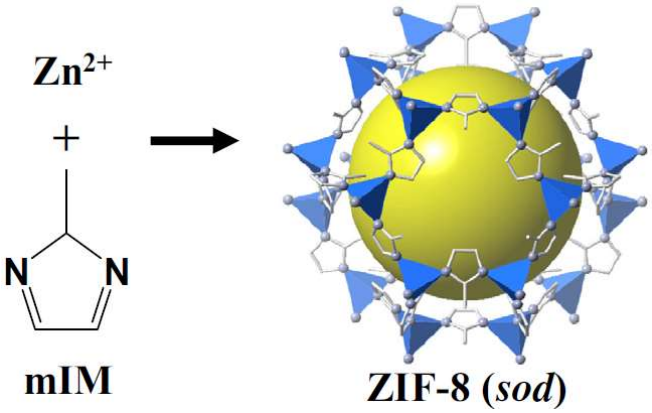

Figure 1.10 The crystal structure of ZIF-8: Zn (polyhedral), N (sphere), and C (line)[47]

The direct carbonization of ZIF-8 into nitrogen-rich porous carbon has been widely reported.[49-58] ZIF-8 as a self-sacrificing template, acting as both the carbon and nitrogen sources in a facile carbonization process. The direct implement of nitrogen during synthesis enable the encapsulation of high amount of nitrogen into the carbon framework. The resulting

doi:10.6342/NTU201901225

nitrogen-doped carbon materials (NCs) not only inherited the polyhedral shape of the parent ZIF-8 but also retained rich nitrogen content, high specific surface area and hierarchical porosity with well-conducting networks. The nitrogen atoms on ZIF-8 were converted into pyridinic-N, pyrrolic-N or graphitic-N, as shown schematically in Figure 1.11.[59] Pyridinic-N is regarded as N-6, because the N atom substitutes a carbon atom in the C6 ring and bonds with two sp^2 carbon atoms and as a member of the hexagon, while N-5 representing pyrrolic-N which form five-membered ring pentagon and contributes two electrons to the π system. Graphitic-N is also known as N-Q, which located inside the graphitic carbon plane and act as a substitution for C atom and bonds with three sp^2 carbon atoms.[59,60] Pyridinic-N on NCs could serve as the electrochemical active sites for enhancing the capacitive behaviors.[58,60,61] While graphitic-N could serve as catalytic active sites for aerobic oxidation through the formation of oxygen radicals on N-O_2 adducts.[62-64]

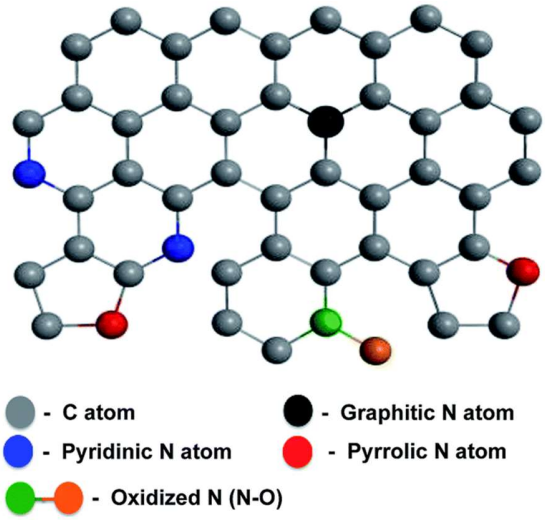

Figure 1.11 The schematic structure of different types of N atoms in NCs[59]

doi:10.6342/NTU201901225

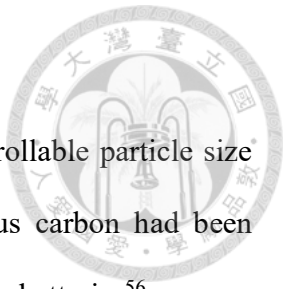

Owing to several advantages, such as high nitrogen loading, controllable particle size and stable porous structure, ZIF-8-derived nitrogen-doped nanoporous carbon had been applied in different fields, including electrochemical[49,51,52,57], lithium-ion batteries[56], oxygen reduction reaction[55,58] and catalytic reaction[50,53]. In previous work by our group, we had demonstrated nitrogen-doped carbon as the first metal-free catalyst for the aerobic oxidation of 5-hydroxymethylfurfural (HMF) to 2,5-furandicarboxylic acids (FDCA) by using ZIF-8-derived nitrogen-doped nanoporous carbon.[54] FDCA yield of 80% was achieved by using this efficient heterogeneous catalyst.

doi:10.6342/NTU201901225

2. Literature review

A conventional route for MA production was via furfural oxidation by either gas phase or liquid phase media. The liquid phase catalytic oxidation of furfural was first demonstrated by Yin's group, with O_2 and phosphomolybdic acid catalyst in a water/tetrachloroethane biphasic system.[65] Under optimized conditions (i.e. under 20 atm of O_2, at 383 K for 14 hours), the furfural conversion was 50.4% and the selectivity to maleic acid was 69% (i.e. 34% yield). In this biphasic system, the oxidation reaction occurred in the aqueous phase, while the organic phase served as a reservoir to gradually release the substrate through the phase equilibrium. The same research group then reported the combination of phosphomolybdic acid with copper nitrate to selectively oxidize furfural to maleic acid.[66] As a result, 51% selectivity and 95% conversion of furfural (i.e. 48.5% yield) was achieved. However, these reaction system was conducted under a harsh condition, such as high O_2 pressure (20 atm) and more importantly the reusability of these catalysts has not been reported.

In order to enhance the catalytic performance of furfural oxidation to maleic acid, another alternative has been considered. By using the liquid oxidant, hydrogen peroxide (H_2O_2), the MA yield was significantly improved. De Oliveira Vigier and co-workers have reported that 61% of MA could be achieved in a BHC / H_2O_2 system.[67] Betaine hydrochloride (BHC) is a co-product of the sugar beet industry, and it acts as s strong acid, which having pH value about 1 under the studied conditions. The main advantage of betaine hydrochloride (BHC) was that it was recylcable if compare with homogeneous mineral acid. Moreover, it was readily available from biomass. In the previous study carried out in this group, reaction media containing water and BHC were used to produce (i) furfural from hemicellulose and

doi:10.6342/NTU201901225

(ii) 5-hydroxymethylfurfural (HMF) from fructose and inulin. In this system, BHC is capable to produce MA directly from xylose in a one-pot two-step process, thus streamlining the production of important industrial intermediates directly from sugars.

So far, the highest yield of maleic acid produced from furfural was reported by Zhang et al..[68] A metal catalyst-free system was developed in order to avoid the issue of catalyst deactivation. To perform the conversion of furfural to maleic acid, formic acid was used as the homogeneous catalyst in the presence of H_2O_2 as the oxidant. They conclude that in this reaction system, H_2O_2 / furfural ratio of 6 is optimal to achieve the highest yield of MA (95%) at 60 °C. However, an extremely large amount of formic acid has been used, which may cause a bad impact on the environment, and also become a great impediment to the purification process.

The first reported heterogeneous catalyst for this reaction was titanium-silicate 1 catalyst (TS-1).[69] A high yield of MA (i.e. 78%) was achieved under optimized reaction conditions (i.e. 4.6 wt% of furfural, 4.6 wt% of catalyst, an H_2O_2 / furfural mol ratio of 7.5, 323 K for 24 hours reaction). However, the leaking of metal during reaction was observed as the main limitation of this catalyst for practical application in industry. In addition, the production of MA was improved by combining the utilization of solvents and solid catalyst. γ-valerolactone (GVL), a renewable solvent allows the production of furfural from lignocellulose biomass, and direct upgrading of furfural to MA by using titanium silicalite-1 (TS-1) as the catalyst and H_2O_2 as the oxidant.[70] A 70% yield of MA was obtained in GVL-H_2O medium at 70 °C and 6 hours, whereas the highest yield in the only-water reaction media was 55% (2-4 hours). Moreover, the MA yield can also be improved to 83% (10 hours) by creating the mesoporous TS-1 catalyst. GVL, as a co-solvent has improved the yield of MA by preventing the

doi:10.6342/NTU201901225

deposition of by-products over the TS-1 surface and/or within their cavities, thus substantially enhancing the long-term stability of the catalyst. Moreover, they also demonstrated the separation of MA from the product solution by the precipitation of monosodium maleate through neutralization with NaOH.

The summary of the catalyst and reaction conditions for the reported furfural to maleic acid oxidation reaction were listed in Table 2.1. Overall, although these studies show good results on the synthesis of MA from furfural, most of them relying on the utilization of the acidic catalyst which having medium or strong acidity. So far, few reports using heterogeneous catalyst was investigated for furfural oxidation to MA, which led to the lack of general evaluations for fundamental studies and practical applications. Thus, a synthesis process by using a heterogenous acid-free catalyst is greatly required for the consideration of catalyst recyclable and environmentally friendly.

doi:10.6342/NTU201901225

Table 2.1 Summary of the reported furfural to maleic acid reaction

Entry	Catalyst	Oxidant	Solvent	Conditions	MA Yield (%)	Ref.
1	phosphomolybdic acid	O_2 (20 atm)	water / tetrachloroethane	110 °C 14 h	34.5	65
2	$Cu(NO_3)_2$ + phosphomolybdic acid	O_2 (20 atm)	water	98 °C 14 h	48.5	66
3	Betaine hydrochloride (BHC)	H_2O_2	water	100 °C 30 min	61	67
4	formic acid	H_2O_2	formic acid	60 °C 4 h	95	68
5	titanium silicalite	H_2O_2	water	50 °C 24 h	78	69
6	titanium silicalite	H_2O_2	water / γ-valerolactone (GVL)	70 °C 6 h	70	70
				70 °C 10 h	83	70

doi:10.6342/NTU201901225

3. Objectives

Maleic acid (MA) is a useful platform chemical which can be used as a starting material to synthesis high value-added chemicals, and the production of it from furfural has been investigated by a lot of researchers. However, most of the reported reaction system on furfural to maleic acid conversion relying on an acidic catalyst, in which recyclable issue and environmental problem became the main disadvantages. Therefore, in this work, we aim to convert furfural into maleic acid under a mild condition, by using a metal- and acid-free heterogeneous catalyst. With the aid of H_2O_2 as the oxidant, the ZIF-8-derived nitrogen-doped nanoporous carbon playing a critical role as a catalyst for catalyzing the conversion of furfural to maleic acid. Here, we will mainly discuss the catalytic performance of the N-doped carbon for conversion of furfural into MA.

doi:10.6342/NTU201901225

4. Experimental

4.1. Chemicals and materials

Chemical	Formula	Abbreviation	Information
2,5-furandicarboxylic acid	$C_6H_4O_5$	FDCA	Sigma-Aldrich
2-methylimidazole	$C_4H_6N_2$	MeIM	Sigma-Aldrich
5-hydroxymethylfurfural	$C_6H_6O_3$	HMF	Sigma-Aldrich
Acetic acid	CH_3COOH	-	J.T. Baker
Acetone	C_3H_6O	-	Alfa Aesar
Furoic acid	$C_5H_4O_3$	FuA	Sigma-Aldrich
Chitosan	$(C_6H_{11}NO_4)_n$	-	Sigma-Aldrich
Ether	$C_4H_{10}O$		J.T. Baker
Formic acid	CH_2O_2	FA	Sigma-Aldrich
Fumaric acid	$C_4H_4O_4$	FumA	Acros
Furan	C_4H_4O		Sigma-Aldrich
Furfural	$C_5H_4O_2$		Acros
Hydrochloric acid	HCl	HCl	37%, Honeywell
Hydrogen peroxide	H_2O_2	H_2O_2	35% , Acros
Maleic acid	$C_4H_4O_4$	MA	Sigma-Aldrich
Melamine	$C_3H_6N_6$	-	Sigma-Aldrich
Methanol anhydrous	CH_3OH	MeOH	Sigma-Aldrich
Sodium hydroxide	NaOH	NaOH	Honeywell
Succinic acid	$C_4H_6O_4$	SA	Sigma-Aldrich
Sulfuric acid	H_2SO_4	H_2SO_4	Sigma-Aldrich
Urea	NH_2CONH_2	-	Alfa Aesar
Zinc nitrate hexahydrate	$Zn(NO_3)_2.6H_2O$	-	Sigma-Aldrich
Amberlyst-15	$C_{18}H_{18}O_3S$	-	Sigma-Aldrich
Polyvinylpyrrolidone K-30	C_6HNO	PVP K-30	TCI

doi:10.6342/NTU201901225

4.2. Equipment

Equipment	Information
Centrifugator	Sigma, 3-30 KS
Elemental Analyzer	Elementar Vario EL cube
Furnance	Thermolyne
High performance liquid chromatography (HPLC)	JASCO RI-2031 plus detector
Hotplate	Thermal scientific
Lyophilizer	FDU-1200
Oven	DENG YENG Circulator Oven DO45
Rotary evaporator	Eyela oil bath OSB-2000
Scanning electron microscope (SEM)	NovaTM NanoSEM 230
Sonicator	DELTA ultrasonic cleaner
Specific Surface Area & Pore Size Distribution Analyzer	BELSORP-series
Thermogravimetry/differential thermal analysis thermoanalyzer (TG-DTA)	Rigaku Thermo plus2 system TG8210
Tubular furnace	Thermo scientific Lindberg Blue M
X-ray diffraction pattern (XRD)	Rigaku Ultima IV
X-ray photoelectron spectroscopy (XPS)	Thermo Scientific, Theta Probe

doi:10.6342/NTU201901225

4.3. Preparation of catalyst

4.3.1. Synthesis of ZIF-8-derived N-doped carbon material

Nitrogen-doped nanoporous carbons were synthesized according to the previous literature with slight modification.[54] Here, polyvinylpyrrolidone (PVP) was used as the structure directing agent and surface modifier of ZIF-8 nanoparticles, thus an organic phase synthesis (i.e. methanol system) of ZIF-8 from $Zn(NO_3)_2 \cdot 6H_2O$ and 2-methylimidazole (MeIM) with excess PVP would produce uniform polyhedron shaped ZIF-8 nanoparticles. Typically, 2-methylimidazole (4.2 g, 0.0511 mol) and polyvinylpyrrolidone (PVP K-30, 12 g) was dissolved into methanol (150 mL). The solution was stirred thoroughly until well dispersion to form a clear solution. On the other side, $Zn(NO_3)_2 \cdot 6H_2O$ (4.4 g, 0.0147 mol) was dissolved in methanol (150 mL), and the mixture was then added into the 2-methylimidazole solution dropwise with stirring at the same time. The solution was further stirred for 1 hour and turned into a white solution. After aging for 24 hours without any interruption at room temperature, a white precipitate of ZIF-8 formed. The white solid was recovered from the milky colloidal solution by centrifugation and washed several times with methanol to remove 2-methylimidazole residues. Finally, the powder was dried and activated before used in the catalytic reaction.

doi:10.6342/NTU201901225

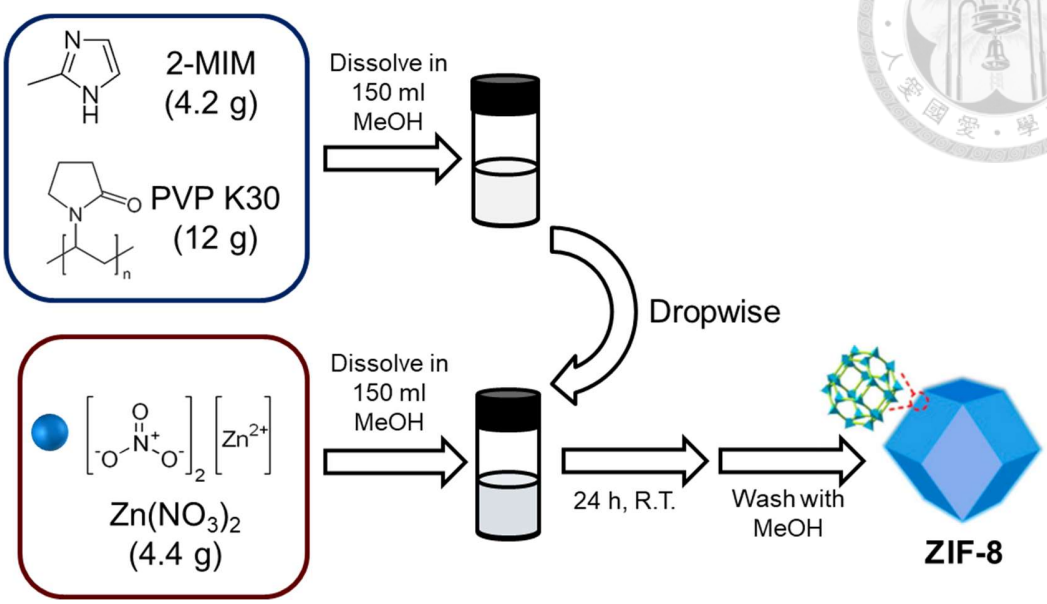

Figure 4.1. Synthesis procedure of ZIF-8 materials

Next, the as-synthesized ZIF-8 powders were placed into a tubular furnace under flowing N_2 atmosphere, and calcined at given temperatures (600, 700, 800, and 900 °C) for 8 hours with a heating rate of 5 °C min^{-1}. After carbonization, the samples were washed thoroughly with concentrated HCl (36.5%) to remove the residual zinc components. Finally, the resulting samples were purified by washing with deionized water and methanol for several times and activated at 150 °C for 5 hours the catalytic reaction. The samples were named to be NC-*x*, where *x* represents the calcination temperature of 600, 700, 800, and 900 °C respectively.

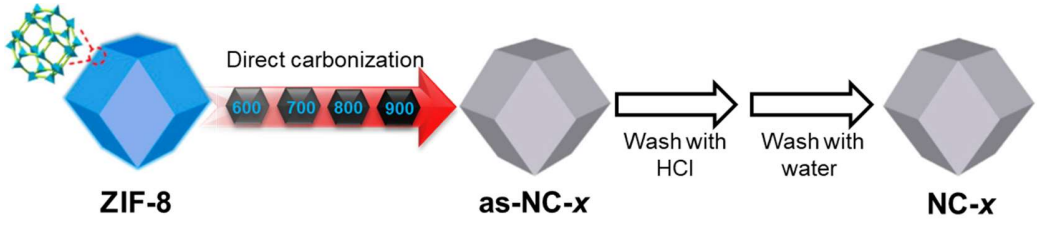

Figure 4.2. Typical procedure of ZIF-8 carbonization to NC-*x*

doi:10.6342/NTU201901225

4.3.2. Synthesis of melamine-derived N-doped carbon

Graphitic carbon nitride was synthesis according to literature.[71] The melamine powder (10 g) was placed in a crucible with covered and heated at 520 °C for 4 hours with a heating rate of 10 °C / min in air. After completion of the reaction, the furnace was cooled to room temperature. The yellow-colored powder was collected and used in the described experiments.

4.3.3. Synthesis of biomass-derived N-doped carbon

The nitrogen-doped carbon materials from biomass were synthesis according to literature with slight modification.[72] Typically, urea (12 g) was first dissolved in water (10 mL), chitosan (1 g) was then added slowly to the urea solution with vigorous stirring. After the complete dispersion of chitosan, acetic acid (500 μL) was added quickly with vigorous stirring for 30 minutes to achieve a homogeneous semi-transparent paste. After drying at 70 °C overnight, a single block of white solid was obtained. Slow pyrolysis was carried out at 900 °C for 5 hours under N_2 atmosphere, with a heating rate of 3 °C / min.

doi:10.6342/NTU201901225

4.4. Furfural to maleic acid reaction

The aerobic oxidation of furfural to maleic acid was carried out in a 25 mL round bottom flask fitted with a reflux condenser to prevent the loss of solvent by evaporation. Typically, furfural (1 mmol; 0.083 mL), catalyst (0.05 g), were added into a 25 mL three-neck flask containing 5 mL of solvent. The reaction mixture was then placed in an oil bath which was preheated. After reaching the desired reaction temperature, hydrogen peroxide (5 mL) was added, and the reaction time was started at this moment. Under magnetic stirring, the reaction mixture was stirred for given reaction time at given reaction temperature. After the reaction time, the product solution was cooled to room temperature and diluted into 25 mL with deionized water. The solution was filtered with a syringe filter (0.22 μm pore size) and prepare for HPLC analysis.

doi:10.6342/NTU201901225

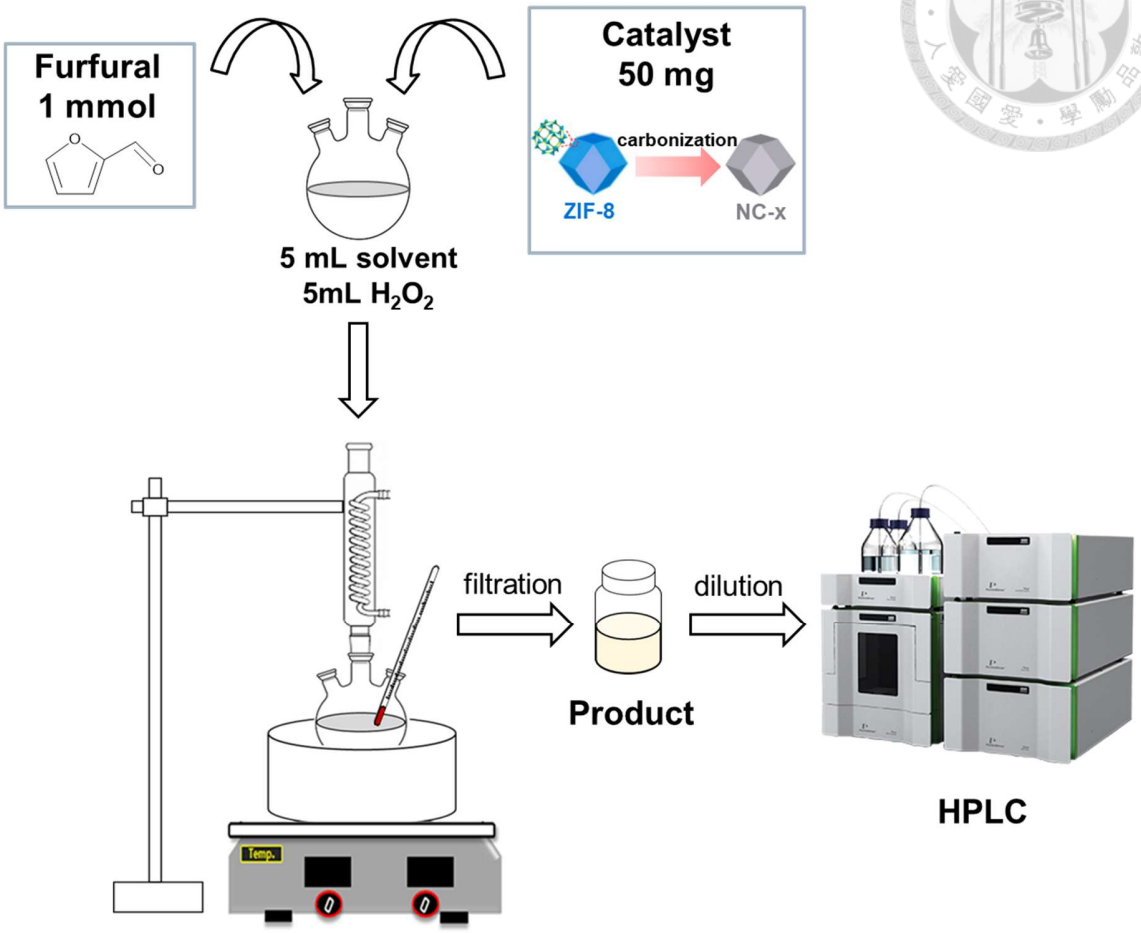

Figure 4.3. Furfural to maleic acid reaction process

doi:10.6342/NTU201901225

4.5. Characterization of products

After the reaction, the reaction solution was separated from the solid catalyst by centrifugation and syringe filtration (0.22 μm pore size). An external standard calibration curve was utilized to calculate the concentration of furfural and all products that were quantified with HPLC beforehand (an ICE-Coregel 87H3 column; operation at 35 °C). The mobile phase was 8 mM sulfuric acid aqueous solution at a flow rate of 0.6 mL min^{-1}. The retention time is 8.6 min for maleic acid, 12.54 min for succinic acid, 14.3 min for formic acid, 15.8 min for fumaric acid, 18.25 min for 5-hydroxy-2(5H)-furanone, 32.29 min for 2(5H)-furanone, 35.8 min for 2-furoic acid, and 56.9 min for furfural.

The conversion *X* and products yield *Y* are calculated by the following formula, where [ ] is the concentration.

$$\mathrm{X}\ (mol\%) = \frac{[furfural]_{initial} - [furfural]_{final}}{[furfural]_{initial}}$$

The yield of products in the solution is calculated to be:

$$Y_i\ (mol\%) = \frac{([product]_i)_{formed}}{[furfural]_{initial}}$$

doi:10.6342/NTU201901225

4.6. Characterization of catalyst

4.6.1. Scanning electron microscope (SEM)

The morphology of the samples was observed with SEM (Nova^{TM} NanoSEM). All the samples were taped on the carbon tape. The samples before SEM observation were kept under vacuum to remove the moisture content.

4.6.2. X-ray diffractometer (XRD)

Wide-angle patterns of powder X-ray diffraction pattern (XRD) were measured on Rigaku Ultima IV with Cu Kα radiation (λ=1.5418 Å) to check the crystallinity.

4.6.3. Specific Surface Area & Pore Size Distribution Analyzer

The nitrogen adsorption / desorption isotherm was measured with BELSORP-series. The specific surface area and pore size distribution were evaluated correspondingly.

4.6.4. Elemental analyzer (EA)

The chemical composition of samples (i.e., carbon, nitrogen and hydrogen) was analyzed with elementar Vario EL cube. (for NCSH, German)

4.6.5. X-ray photoelectron Spectroscopy (XPS)

The chemical state of nitrogen (i.e. N 1s) was performed on an X-ray photoelectron spectroscopy. (XPS, Thermo Scientific, Theta Probe).

doi:10.6342/NTU201901225

4.7. Product purification

In order to obtain a pure maleic acid product, a purification procedure was developed. NaOH was added to precipitate the carboxylic acids to become carboxylate salts. An exact amount of NaOH (number of moles of NaOH / MA = 1) was added in order to precipitate only the most acidic proton of the MA. Ether was used to extract the remained acid products which are undesired. Then, by adding a strong acid, sodium maleate salt was transformed back to maleic acid. Lastly, acetone was added to remove the co-product, NaCl.

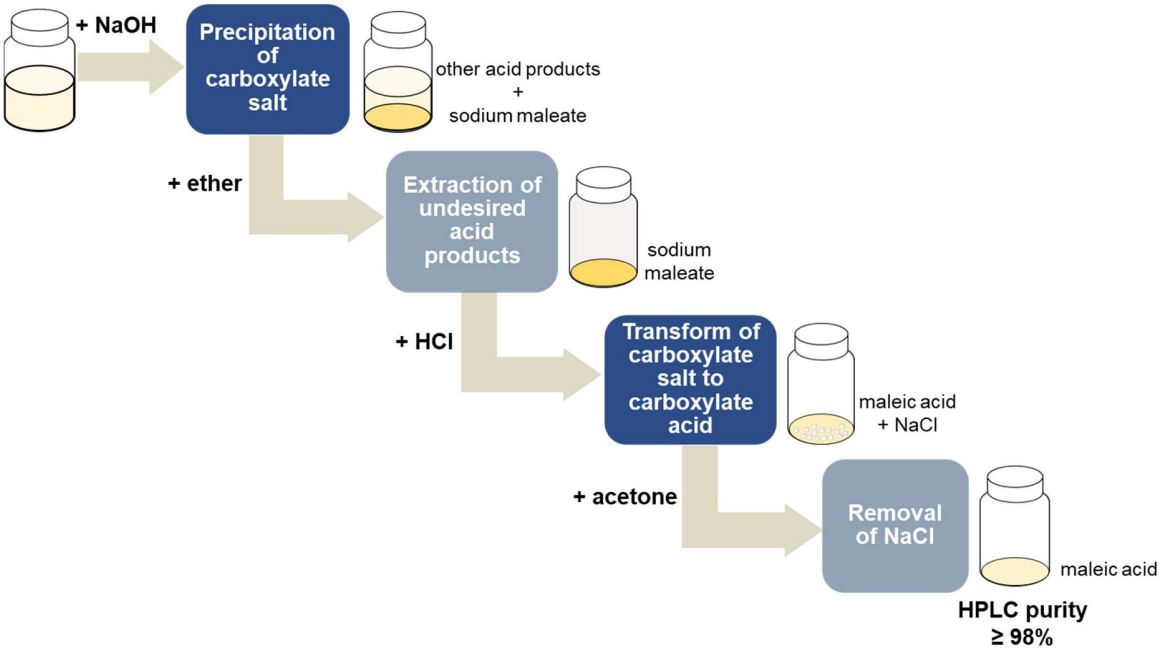

Figure 4.4. Product purification process

doi:10.6342/NTU201901225

5. Results and Discussion

5.1. Materials Characterization

5.1.1 SEM analysis

The morphology of the synthesized parent ZIF-8 and the NC materials were analyzed by scanning electron microscope (SEM), and the SEM image of the synthesized ZIF-8 and NC-*x* were shown in Figure 5.1 and Figure 5.2 respectively. It can be observed that ZIF-8 crystals possess typical rhombic dodecahedron shape with a smooth surface and well dispersion. The average diameter is about 150-200 nm. And all of the as-synthesized N-doped carbon materials (i.e. NC-600, NC-700, NC-800, and NC-900) inherited the original morphology of the ZIF-8 particles, even after high-temperature thermal treatment under a N_2 atmosphere. However, after carbonization and washing with HCl, the surfaces of the carbon samples became rough, and the particles also shrinkage and aggregate.

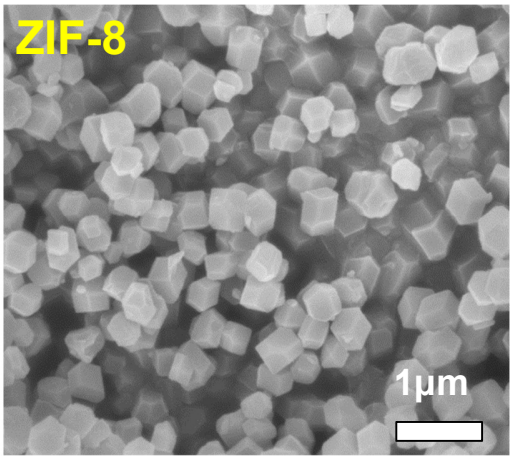

Figure 5.1 SEM image of the synthesized ZIF-8 particles

doi:10.6342/NTU201901225

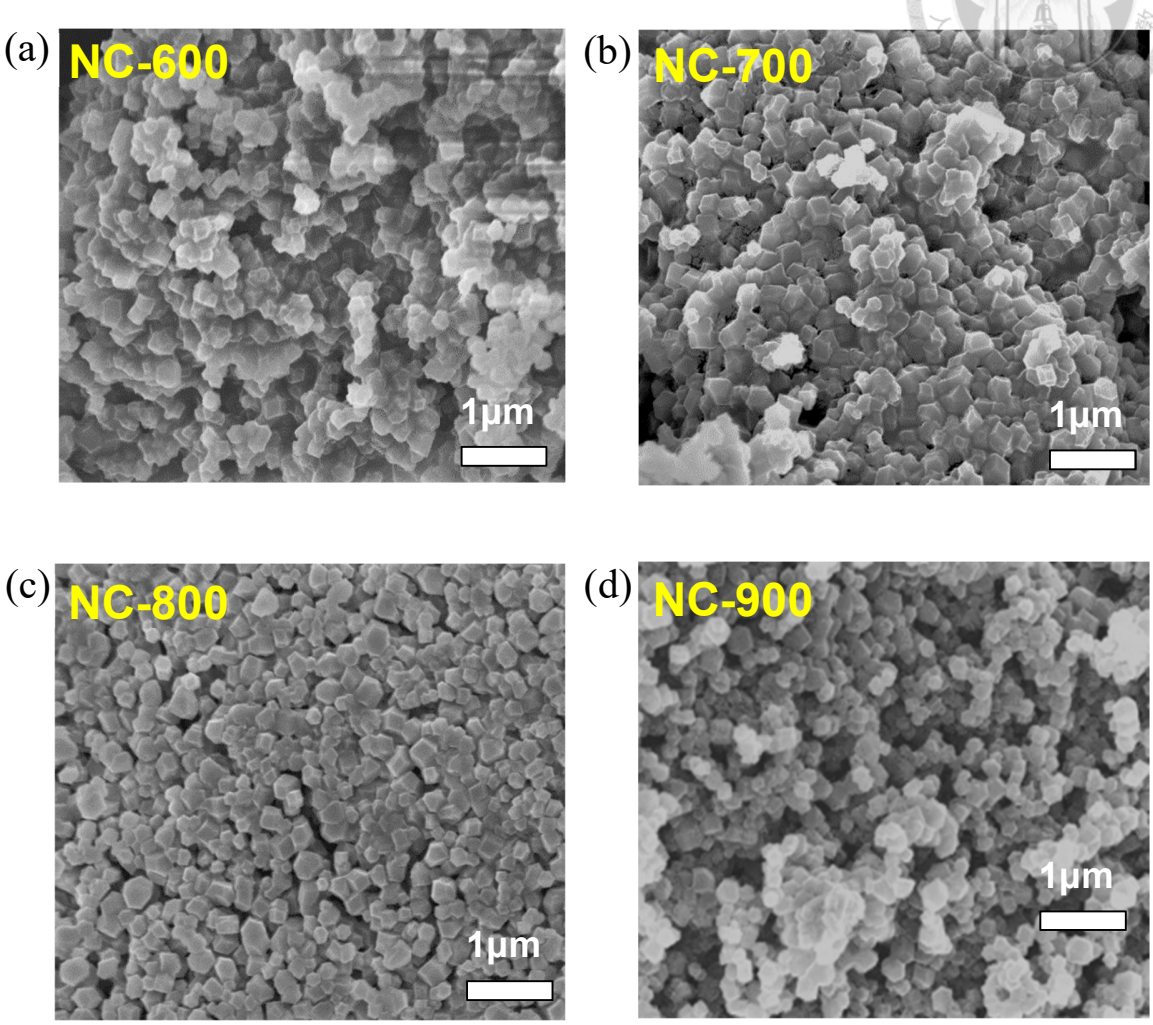

Figure 5.2 SEM image of the synthesized NC-*x*

(a) NC-600 (b) NC-700 (c) NC-800 (d) NC-900

doi:10.6342/NTU201901225

5.1.2 XRD analysis

The crystalline structure of the synthesized ZIF-8 and NC-*x* were characterized with X-ray diffraction (XRD). Figure 5.3 shows the XRD pattern of the synthesized ZIF-8. All diffraction peaks match well with the simulated data reported in the literature. The XRD pattern of NC-*x* was shown in Figure 5.4. All of the as-synthesized N-doped carbon materials (i.e. NC-600, NC-700, NC-800, and NC-900) exhibited similar diffraction features with a broad peak at approximately 24°, corresponding to the carbon (002) peak, which indicates that ZIF-8 has been successfully converted into carbon materials after high-temperature pyrolysis. Moreover, the absence of any characteristic peaks indicates that the Zn species have been removed during the process of high-temperature pyrolysis and the following acid wash. Along with the increasing of pyrolysis temperature, the (002) peak become relatively stronger with slight positive shifts, and an additional peak at 44° appeared in NC-900. These phenomena are attributed to the fact that higher pyrolysis temperature can promote higher graphitization degree of the carbon materials.

doi:10.6342/NTU201901225

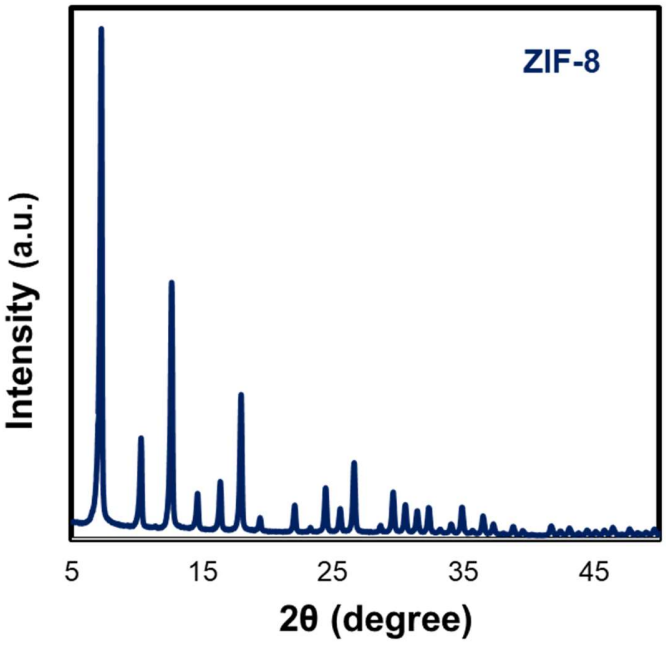

Figure 5.3 XRD pattern of the synthesized ZIF-8 particles

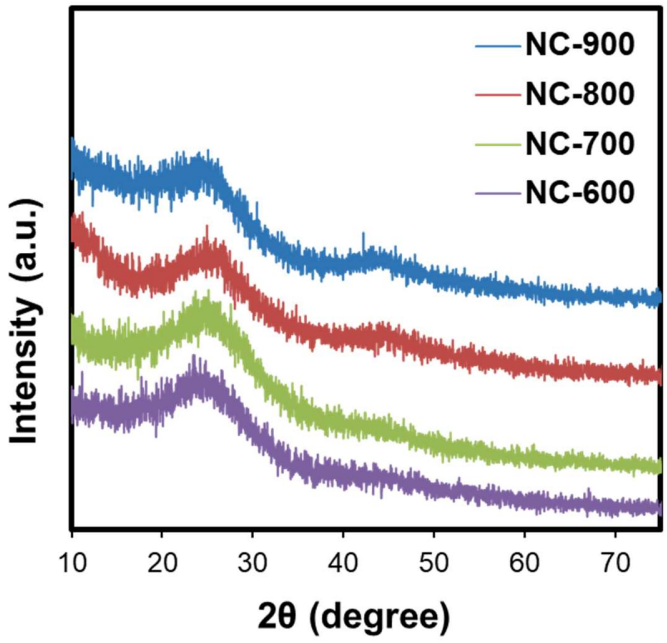

Figure 5.4 XRD pattern of the synthesized NC-*x*

doi:10.6342/NTU201901225

5.1.3 Specific surface area analysis

The pore specific surface area and pore size distribution of the synthesized ZIF-8 and NC-*x* materials were analyzed by the nitrogen adsorption and desorption measurement as shown in Figure 5.1. The NC-*x* materials showed typical Type-I isotherms with sharp uptakes at low relative pressure ($P/P_0 < 0.015$) but a large hysteresis loop at high relative pressure ($P/P_0 > 0.85$), suggesting the intrinsic micropore characteristic with a portion of meso/macropores caused by the sorption of inter-nanoparticle voids. In Table 5.1, we had summarized the pore characteristic of ZIF-8 and NC-*x*. Both micropore and mesopore volumes are exhibited in the materials. The surface areas calculated by the Brunauer-Emmett-Teller (BET) method are 1428, 601, 795, 833, and 813 $m^2 g^{-1}$, for ZIF-8, NC-600, NC -700, NC-800, and NC-900, respectively. Compared with the synthesized ZIF-8, the obtained NC-*x* materials exhibited a significant decrease in the specific surface area. The pore size distribution (derived using the non-local density functional theory (NL-DFT) method) also shifts from 1.2 to 0.59 nm. This could be explained by the collapsed of ZIF-8 frameworks at the high carbonization temperatures, causing the shrinkage of carbon frameworks and the destruction of the well-ordered channel system.

doi:10.6342/NTU201901225

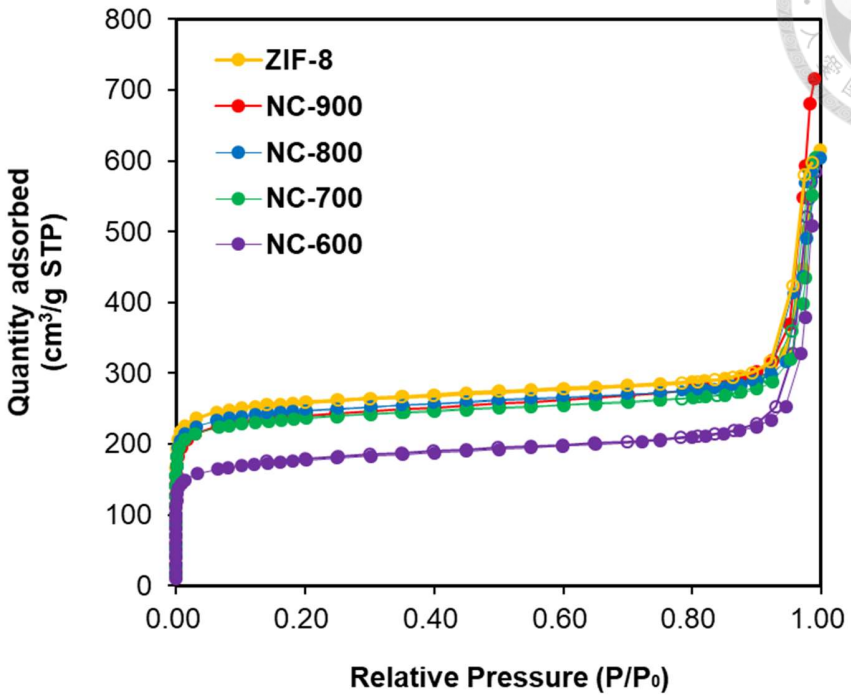

Figure 5.1 Adsorption and desorption isotherms of the synthesized ZIF-8 and NC-*x*

Table 5.1 Pore characteristic of ZIF-8 and NC-*x*

Materials	Specific surface area (m^2/g) [a]	Pore size (nm) [b]	Micropore volume (cm^3/g) [c]	Mesopore volume (cm^3/g) [d]
ZIF-8	1428	1.2	0.17	0.85
NC-600	601	0.59	0.26	0.65
NC-700	795	0.59	0.35	0.58
NC-800	833	0.59	0.29	0.65
NC-900	813	0.59	0.35	0.76

[a]: Specific surface area is calculated with BET theory.
[b]: Pore size is calculated with NLDFT model assuming slit carbon pores.
[c]: Micropore volume is calculated with t-plot value.
[d]: Mesopore volume is the difference of single pore volume and t-plot micropore volume

doi:10.6342/NTU201901225

5.1.4 Elemental analysis (EA)

Elemental analysis was carried out to analyze the elemental composition in the NC-*x* materials. The summary of element composition in Table 5.2 validates that carbon and nitrogen elements are the main compositions for NC-*x*. It can be observed as the calcination temperature for ZIF-8 increased from 600 to 900 °C under the same 8 hours carbonization, the carbon content gradually increases from 44.19% to 63.59%. In contrast, the nitrogen content shows a decrease in amount, where the proportions of nitrogen were calculated to be 24.94 wt% (NC-600), 23.71 wt% (NC-700), 22.47 wt% (NC-800), and 14.29 wt% (NC-900), respectively. This phenomenon could be explained by the collapse of nitrogen-containing 2-imidazole groups in ZIF-8 when the framework destroyed at high temperature, and at the same time the nitrogen contents have been carried off by the airflow.

Table 5.2 The composition of the synthesized NC-*x* materials

Materials	Elemental analysis (wt%)		XPS N 1s (%)		
	N	C	Pyridinic-N (N-6)	Pyrrolic-N (N-5)	Graphitic-N (N-Q)
NC-600	24.94	44.19	89.3	6.16	4.5
NC-700	23.71	47.85	58.52	32.78	8.7
NC-800	22.47	55.63	61.98	23.66	14.37
NC-900	14.29	63.59	47.56	27.6	24.84

doi:10.6342/NTU201901225

5.1.5 X-ray Photoelectron spectroscopy (XPS)

In order to understand the details of the contents and band structures of nitrogen in all the NC-*x* materials, we analyzed the X-ray photoelectron spectroscopy (XPS). From Figure 5.2 and Table 5.2, we can know that the N 1s peak can be deconvoluted to three individual component peaks, representing pyridinic-N (N-6) at 398.4 ± 0.2 eV, pyrrolic-N (N-5) at 399.8 ± 0.2 eV, and graphitic-N (N-Q) at 401.1 ± 0.2 eV. For all the NC-*x* materials, the N-6 was predominant, account for 47.56% - 89.3%, which was in agreement with the results from other studies that the formation of N-6 is preferred at higher overall nitrogen content. This could be explained by the low heat formation of pyridinic group at higher nitrogen content.

Notably, the amount of the N-Q increased drasticallty from 4.5% to 24.84% as the calcination temperature increased from 600 to 900 °C. This could be explained by the thermal unstable nature of N-5, causing them to convert into N-Q more easily at higher temperature. These results suggested that by adjusting the carbonization temperature and time, one can easily control the nitrogen doping level of the resulting materials.

doi:10.6342/NTU201901225

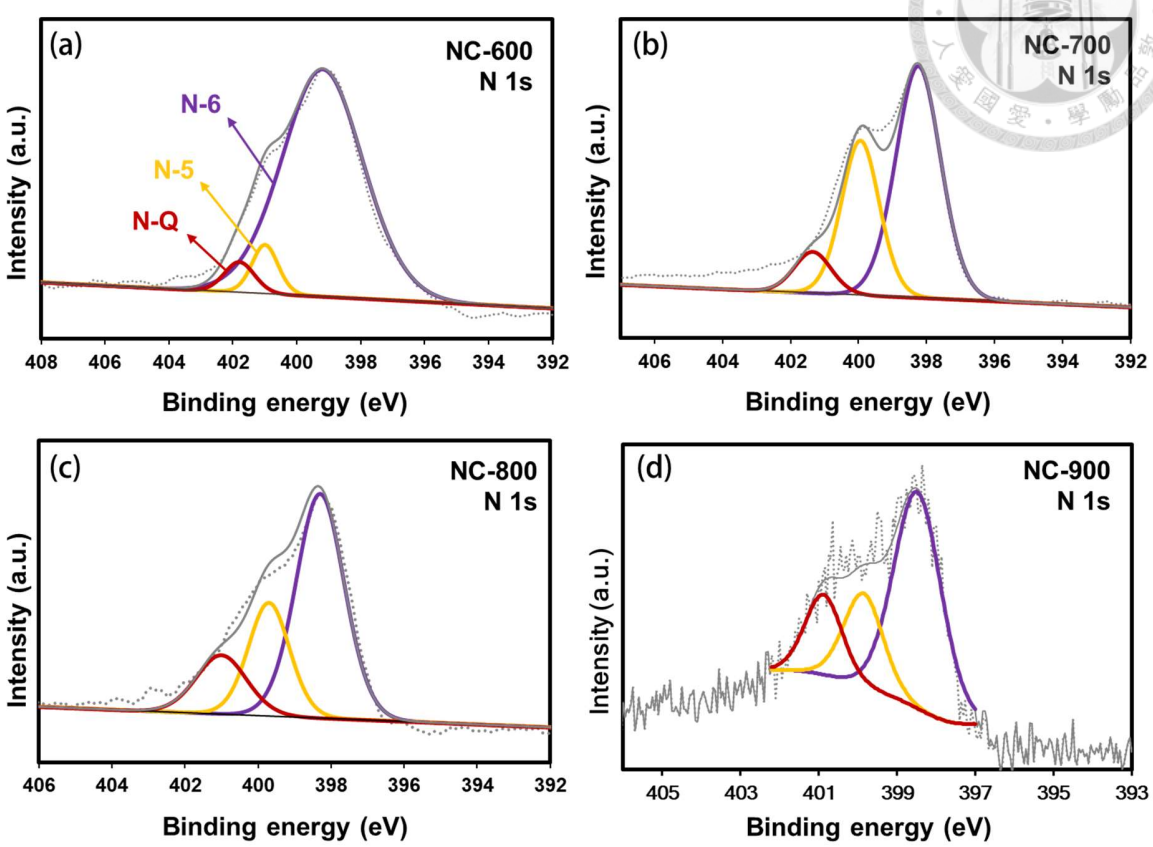

Figure 5.2 XPS pattern of the synthesized NC-*x*

(a) NC-600 (b) NC-700 (c) NC-800 (d) NC-900

doi:10.6342/NTU201901225

5.2. Reaction optimization

A study of the effect of different operating variables on the catalytic behavior was performed. The aim is to find out the best reaction conditions to obtain the highest MA yield. To optimize the reaction conditions, several parameters including catalyst, solvent, H_2O_2 concentration, reaction temperature, and reaction time were investigated.

5.2.1. The effect of catalyst

First of all, a control group with the absence of catalyst was carried out. A 100% of furfural conversion was achieved, with 15% yield of maleic acid in 5 hours. The amount of succinic acid produced was as high yield as MA, indicating that the catalytic oxidation of furfural has two competitive products, including both maleic acid and succinic acid. Then, the furfural oxidation reaction was carried out by using NC-600, NC-700, NC-800, and NC-900, respectively, as the catalyst. The results were shown in Figure 5.3. In 5-hours reaction time, a 100% furfural conversion was achieved in all case, and it was observed that the MA yield has a positive correlation with the carbonization temperature for the ZIF-8 materials. The MA yield in 5 hours was 40%, 53%, 58%, and 61% by using NC-600, NC-700, NC-800, and NC-900, respectively. Moreover, the yield of succinic acid was relatively low (< 9%). These results indicate that NC-*x* catalysts were highly active in converting furfural to MA, and NC-900 was selected as the catalyst for the following optimization of reaction parameters.

doi:10.6342/NTU201901225

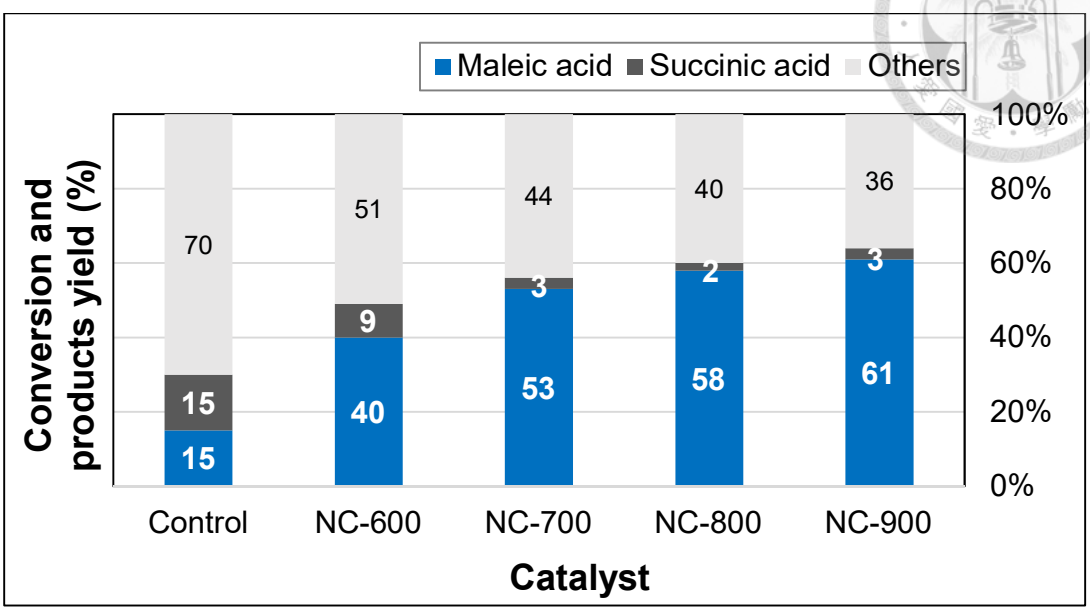

Figure 5.3 The effect of catalyst on furfural to maleic acid reaction

(Reaction conditions: Furfural 1 mmol, catalyst 50 mg, H_2O_2 35 wt% 5 mL, H_2O 5 mL, 80 °C, 5 h)

In order to investigate the relationship between the carbonization temperature of material with the MA yield, we plot the amount of each nitrogen type (i.e. pyridinic-N (N-6), pyrrolic-N (N-5), and quaternary-N (N-Q)) in each NC-*x* materials, respectively. And then we correlate these amount with the MA yield obtained. The plot of the wt% of graphitic-N, pyridinic-N and pyrrolic-N in NC-*x* materials versus the MA yield, respectively, were shown in Figure 5.4, Figure 5.5, and Figure 5.6. It was clearly shown that the MA yield increase linearly with the amount of N-Q content. However, there are no connections between MA yield with N-6 and N-5. This showing that the N-Q site was playing a crucial role in the oxidation reaction, due to the enhanced of reaction rate. We proposed that the mechanism of the aerobic oxidation reaction is also through a radical process, which similar to the reported literature[73]. According to the literature[73,74], the N-Q atoms was acting as electronic promoters

doi:10.6342/NTU201901225

to stimulate the chemical reactivity of the adjacent carbon atoms and promote the formation of oxygen radicals after reacting with the oxidant, such as hydrogen peroxide. They demonstrated that the incorporation of the nitrogen dopants will induce the charge redistribution, and the nitrogen atom having one more electron than carbon will bear a negative charge. Thus, nitrogen atom is not able to host the peroxide species because of the high negative charge. Instead, the carbon atoms adjacent to the N-Q dopants (i.e. *ortho*-carbon) possess a substantially higher positive charge, in which the reactive peroxide species will be more likely to adsorb on its (Figure 5.7).

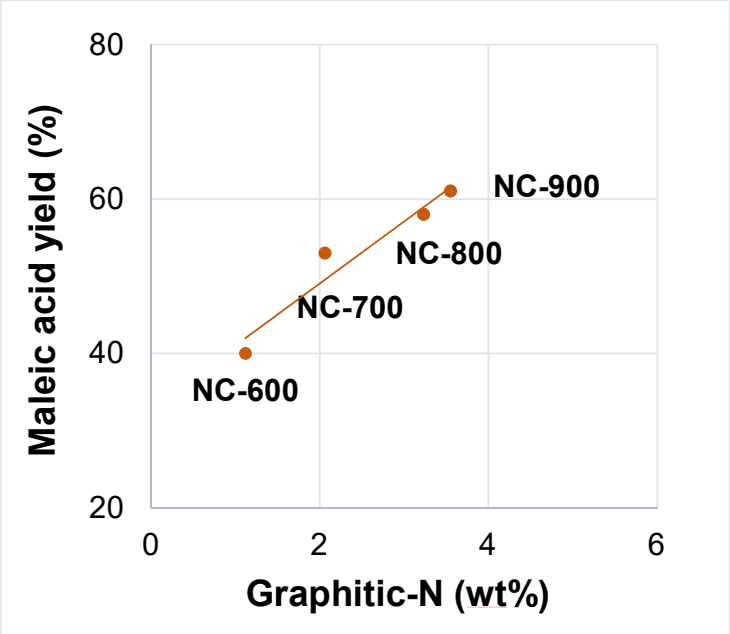

Figure 5.4 The plot of graphitic-N amount on NC-*x* versus MA yield

doi:10.6342/NTU201901225

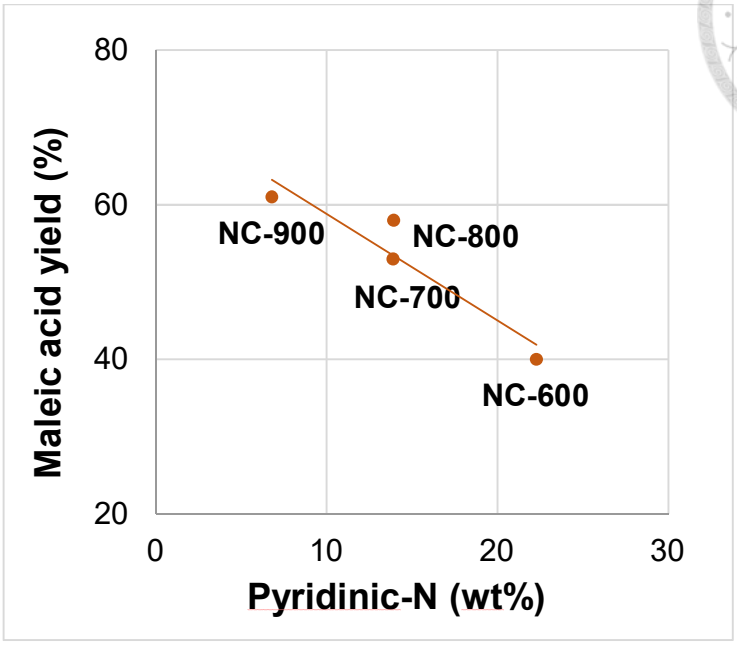

Figure 5.5 The plot of pyridinic-N amount on NC-*x* versus MA yield

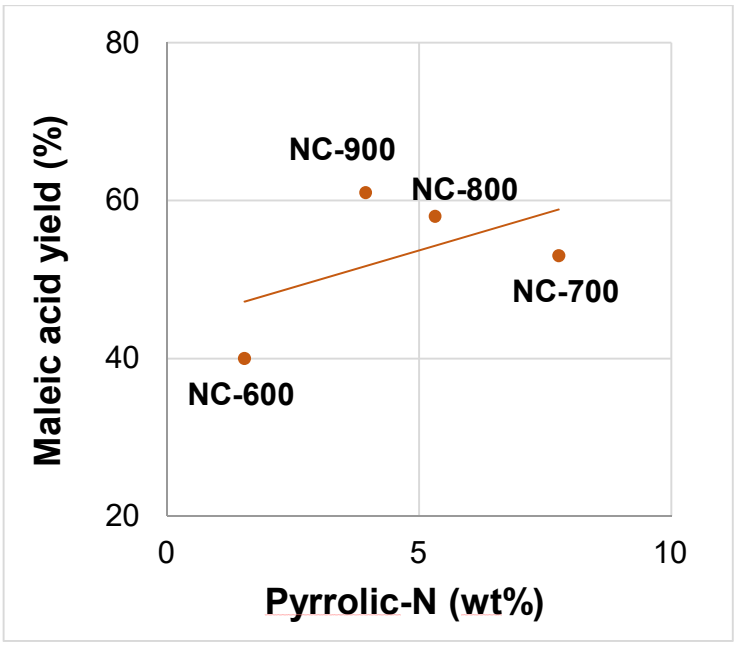

Figure 5.6 The plot of pyrrolic-N amount on NC-*x* versus MA yield

doi:10.6342/NTU201901225

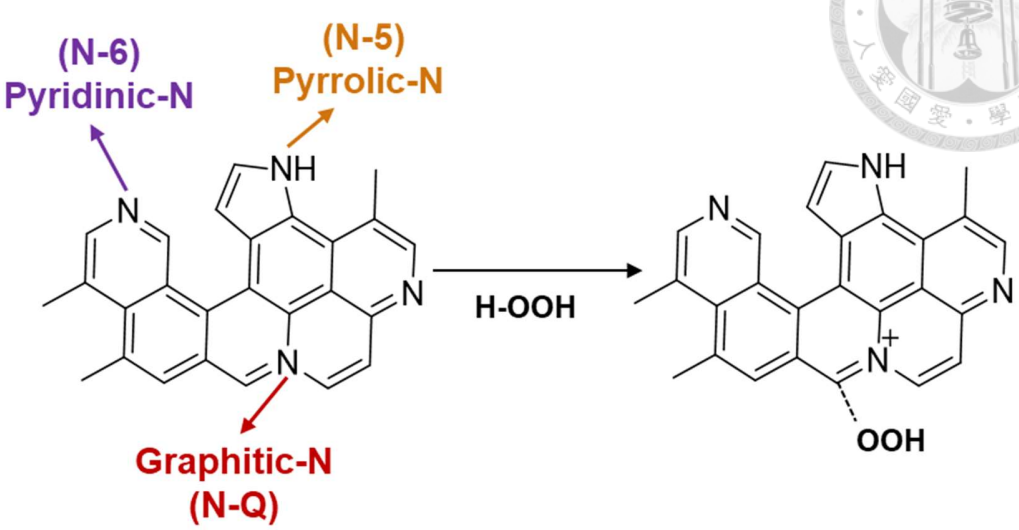

Figure 5.7 Schematic of the absorption of peroxide on *o*-carbon near N-Q sites

In order to prove this hypothesis, we conducted the furfural oxidation reaction in the presence of anti-radical agent, under the same reaction conditions. Gallic acid, which exhibited three hydroxyl groups bonded to the aromatic ring in the *ortho* position, was reported as an excellent anti-radical agent.[75] Thus, 2 mmol of gallic acid was incorporated into the reaction mixture with vigorous stirring to form a uniform solution with well dispersion. The comparison of the results between the reaction with or without adding anti-radical agent was shown in Figure 5.8. It was noted that after the incorporation of the anti-radical, gallic acid, the maleic acid yield shows a significant decrease. At 1 hour reaction time, the MA yield only reached 8%. The further prolong of reaction time only lead to a slight increase in the yield. At 5 hours reaction time, the MA yield was recorded as 34%. The difference in the results indicate that the reaction was greatly inhibited after the addition anti-radical agent. This prove our assumption that the reaction system was proceed through a radical process.

doi:10.6342/NTU201901225

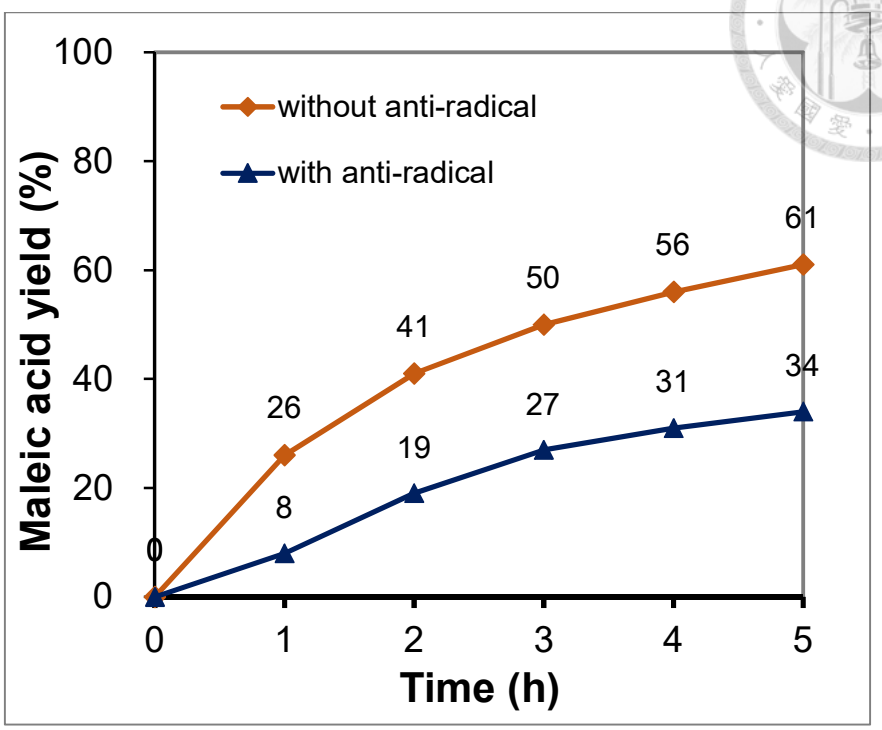

Figure 5.8 The time-dependent analysis before and after incoporation of anti-radical agent (Reaction conditions: Furfural 1 mmol, gallic acid 2 mmol, NC-900 50 mg, H_2O_2 35 wt% 5 mL, H_2O mL, 80 °C)

doi:10.6342/NTU201901225

5.2.2. The effect of solvent

In the previous section, we already determined the appropriate catalyst, which is the NC-900. So next we will focus on the effect of solvent. Solvent usually serves as a medium in which both substrate and solid catalyst suspended, playing important roles in controlling the catalytic activity. Thus, the furfural oxidation reaction was performed in various solvents, including H_2O, dimethylformamide (DMF), dimethyl sulfoxide (DMSO), dimethylamine (DMA), diethylene glycol dimethyl ether (Diglyme), ethanol and N-methyl-2-pyrrolidone (NMP). From Figure 5.9, we can find that all of the organic solvents achieved a high furfural conversion of 98% within 5 hours. However, a very low MA yield was obtained in the range from 2-17%. This result indicates that those solvents were not suitable for furfural oxidation to MA. The highest yield of MA (i.e. 61%) was achieved in the presence of water as a solvent, suggesting that water is the best solvent for converting furfural to MA.

doi:10.6342/NTU201901225

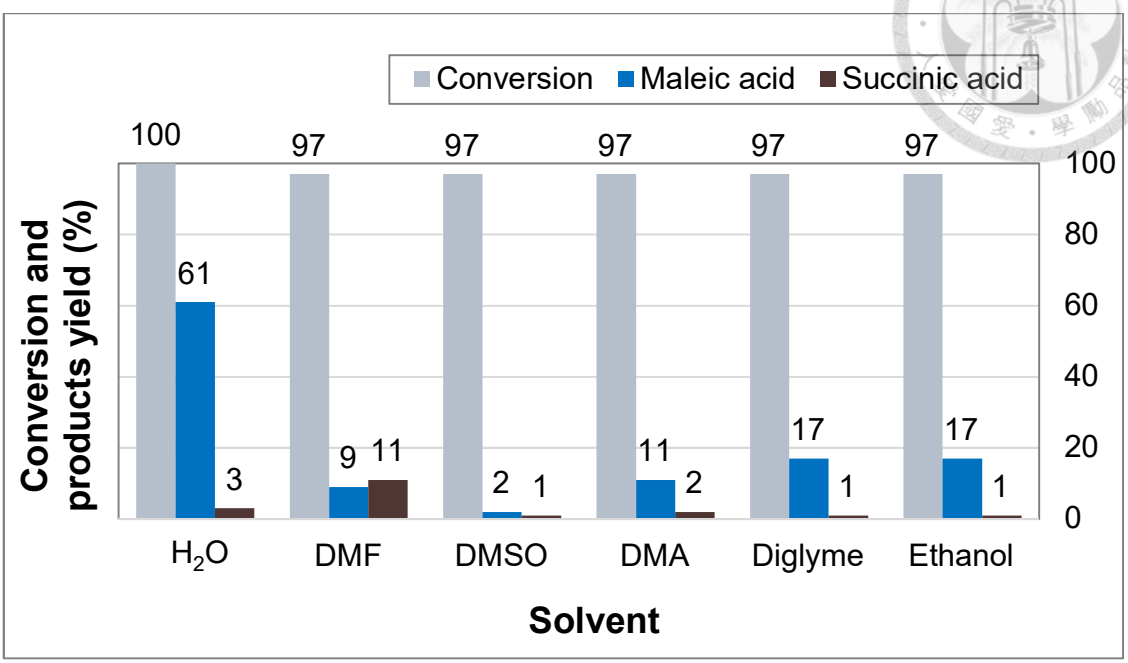

Figure 5.9 The effect of solvent on furfural to maleic acid reaction

(Reaction conditions: Furfural 1 mmol, NC-900 50 mg, H_2O_2 35 wt% 5 mL, solvent 5 mL, 80 °C, 5 h)

5.2.3. The effect of H_2O_2 concentration

The liquid oxidant, hydrogen peroxide (H_2O_2) playing an important role in our reaction system, since it can be decomposed to radical species, which then combine to the active sites of catalyst for catalyzing the reaction. Thus, the effect of H_2O_2 concentration on furfural oxidation has been considered. A different H_2O_2 concentration (i.e. 15%, 20%, 25% and 30%) was tested and the amount of H_2O_2 incorporated was fixed as 5 mL. In fact, there was no formation of MA without the addition of H_2O_2 in the reaction system. Figure 5.10 shown the dependence of MA yield on H_2O_2 concentration. The results shown that the gradual increase of H_2O_2 concentration from 15% to 35% corresponds to the increase of MA yield from 40% to 61%. The highest MA yield of 61% was achieved by using 35% H_2O_2 concentration, where

doi:10.6342/NTU201901225

the rest 36% of other products could be assigned to the intermediate products or side products from decomposition and polymerization of furfural. Thus, we conclude a higher H_2O_2 concentration favor the reaction selectivity towards MA.

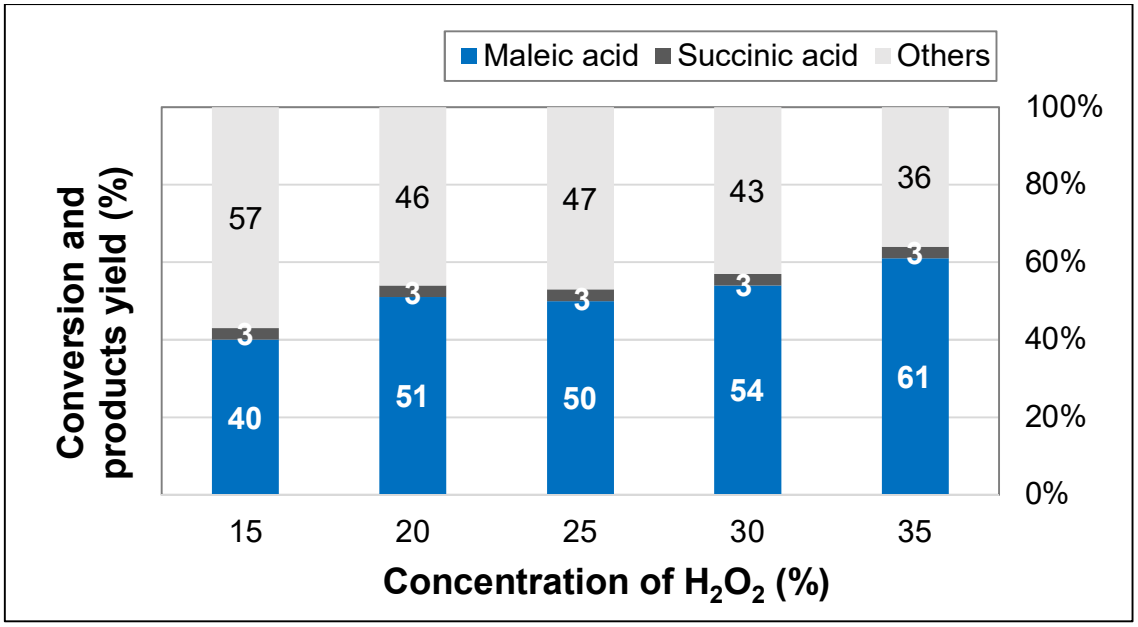

Figure 5.10 The effect of H_2O_2 concentration on furfural to maleic acid reaction (Reaction conditions: Furfural 1 mmol, NC-900 50 mg, H_2O_2 5 mL, H_2O 5 mL, 80 °C, 5 h)

doi:10.6342/NTU201901225

5.2.4. The effect of temperature

In this section, the effect of temperature was investigated. The furfural oxidation was carried out at a different temperature of 40 °C, 60 °C, 80 °C, and 90 °C as shown in Figure 5.11. The results show that the selective catalytic furfural oxidation over NC-900 catalyst was strongly depended on the reaction temperature. Although the furfural conversion in 5 hours are 100% at all tested reaction temperatures, the selectivity towards MA are obviously different. There was only 22% MA yield obtained at 40 °C reaction temperature in 5 hours. This may cause by the slower reaction rate at a lower reaction temperature. When increasing the reaction temperature to 60 °C, the MA yield increase to 47%. Meanwhile, the reaction was carried out at 80 °C, the MA yield reached 61%. However, further increasing of reaction temperature to 90 °C leads to the decrease in MA yield with 54%. This may due to decomposition of furfural and formation of side products at a higher reaction temperature. Moreover, we can also observe more gas bubbles appeared when reaction conducted at 90 °C, and fewer bubbles at 40 °C, indicating the rapid decomposition of peroxide at a higher reaction temperature, which was not favorable for the reaction. Thus, the optimal reaction temperature for furfural oxidation to MA catalyzed by NC-900 catalyst was determined as 80 °C.

doi:10.6342/NTU201901225

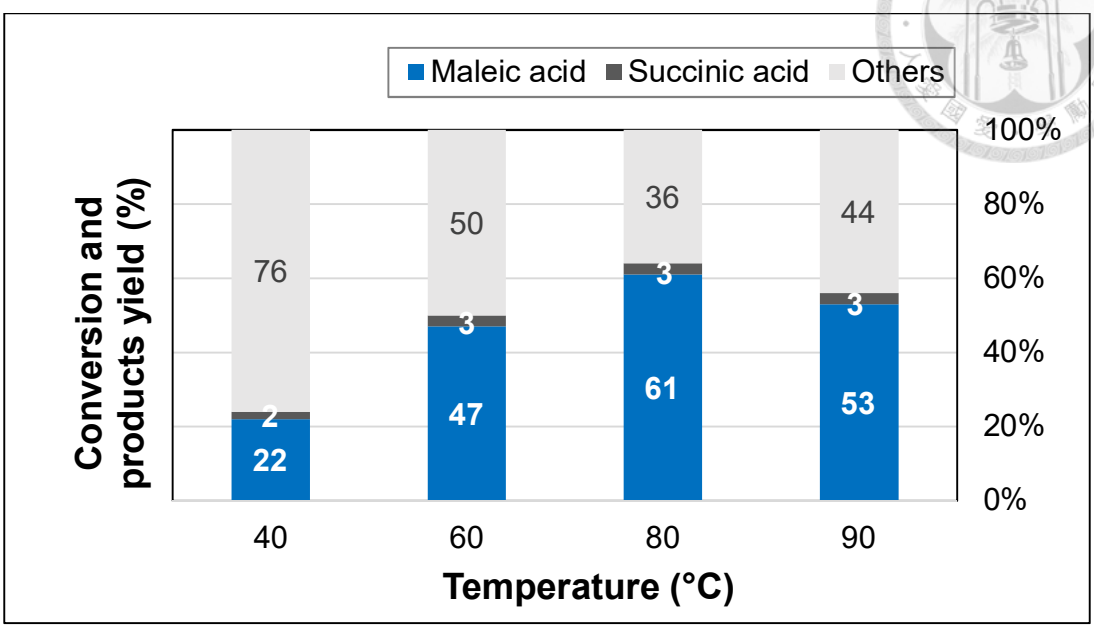

Figure 5.11 The effect of reaction temperature on furfural to maleic acid reaction (Reaction conditions: Furfural 1 mmol, NC-900 50 mg, H_2O_2 35 wt% 5 mL, H_2O 5 mL, 5 h)

5.2.5. The effect of reaction time

The time-dependent analysis was studied by conducting the reaction in time interval as depicted in Figure 5.12. It can be seen in only 1 hour of reaction time, almost all furfural was consumed, in which 97 % conversion of furfural was achieved. A number of products were obtained, but the main products are 5-hydroxy-2(5H)-furanone and MA. A very small amount of succinic acid and 2-furanone was also detected as the side products. Besides, formic acid, 2-furoic acid and fumaric acid were also detected, but their yields were always much lower than 3% (for the sake of simplicity they are not shown in Figure 5.12). The prolong of the reaction time, lead to the remarkably decrease yield of 5-hydroxy-2-furanone, along with the increase of MA yield, all the way from 1 to 5 hours. So, it was suggested that the 5-hydroxy-2(5H)-furanone was converted into MA, and 5-hydroxy-2(5H)-furanone is the

doi:10.6342/NTU201901225

main intermediate in the reaction. A further increase of the reaction time to 6 hours lead to a slight decrease in MA yield, accompanied by the increase of the side products, succinic acid and 2-furanone. Thus, we proposed that 5-hours reaction time was optimum in our reaction system, with NC-900 as a catalyst, assisted with 5 mL of 35% H_2O_2 and conducted at 80 °C.

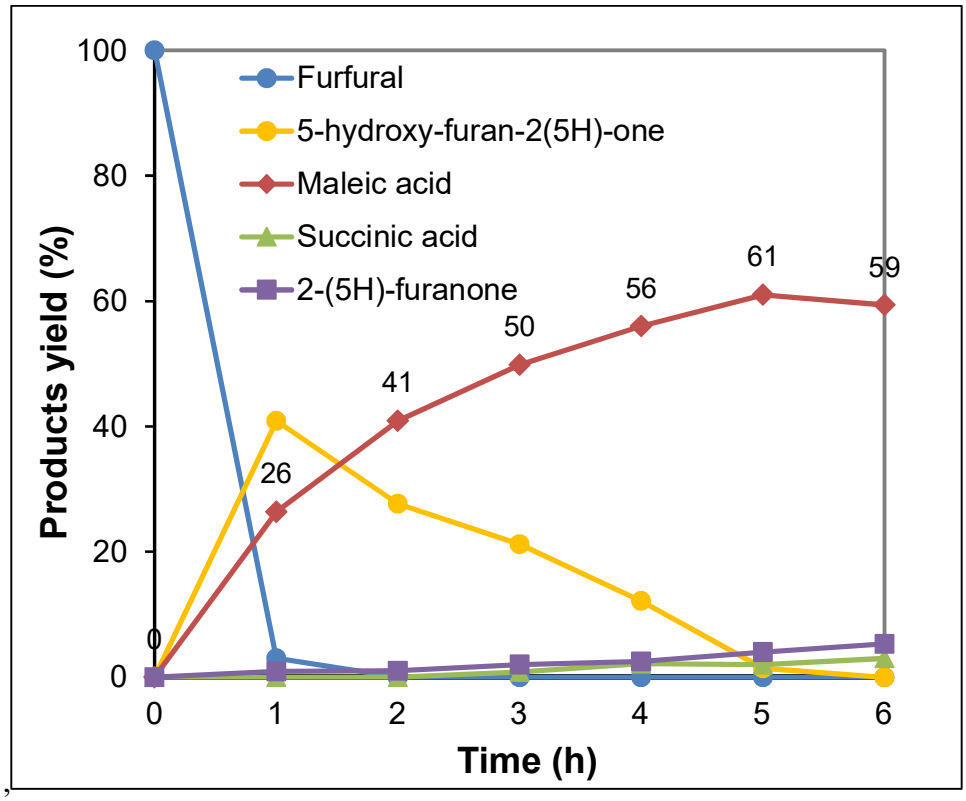

Figure 5.12 The effect of reaction time on furfural to maleic acid reaction (Reaction conditions: Furfural 1 mmol, NC-900 50 mg, H_2O_2 35 wt% 5 mL, H_2O 5 mL, 80 °C)

doi:10.6342/NTU201901225

5.3. Recycle test

Finally, recycle test was performed in order to know the reusability of the catalyst in our reaction. A series of successive runs were conducted. Typically, after a given run of the reaction, the NC-900 catalyst was separated from the reaction mixture by centrifugation, purified by water to remove impurities, and then dried in vacuum. The spent catalyst was then subjected to a calcination treatment in a N_2 atmosphere at 500 °C for regeneration. Then the activated catalyst was used to perform a new reaction run under the same reaction conditions. In Figure 5.13, although the conversion remained unchanged at 100% during the recycle test, the MA yield gradually decreased from 60% at the first time to 38% at the fourth time, suggesting that the catalyst was poisoned under the reaction environment.

To understand the main reason for the catalyst deactivation in our case, the surface of the fresh and spent catalyst was analyzed by XPS (Figure 5.14). As mentioned before, the N 1s configuration of the fresh NC-900 was deconvoluted into three peaks, corresponding to the pyridinic-N (N-6) at 398.4 eV, pyrrolic-N (N-5) at 399.8 eV, and graphitic-N (N-Q) at 401.1 eV. In Table 5.3, it can be noted that the spent NC-900 catalyst exhibited a significant decrease in the amount of N-Q when compare to the fresh NC-900 catalyst, which decrease from 24.84% to 12.2%. And also, these nitrogen species were found to be oxidized after the reaction, leading to the formation of new oxide type bonding (at 402.8 eV). As previously stated, the N-Q species serving as an important site to promote the formation of active peroxide species for enhancing the catalytic performance in our reaction. Thus, we suggest that the decrease in catalytic reactivity during recycle test was due to the decrease in the amount of the N-Q in the NC-900 catalyst after the oxidation reaction.

doi:10.6342/NTU201901225

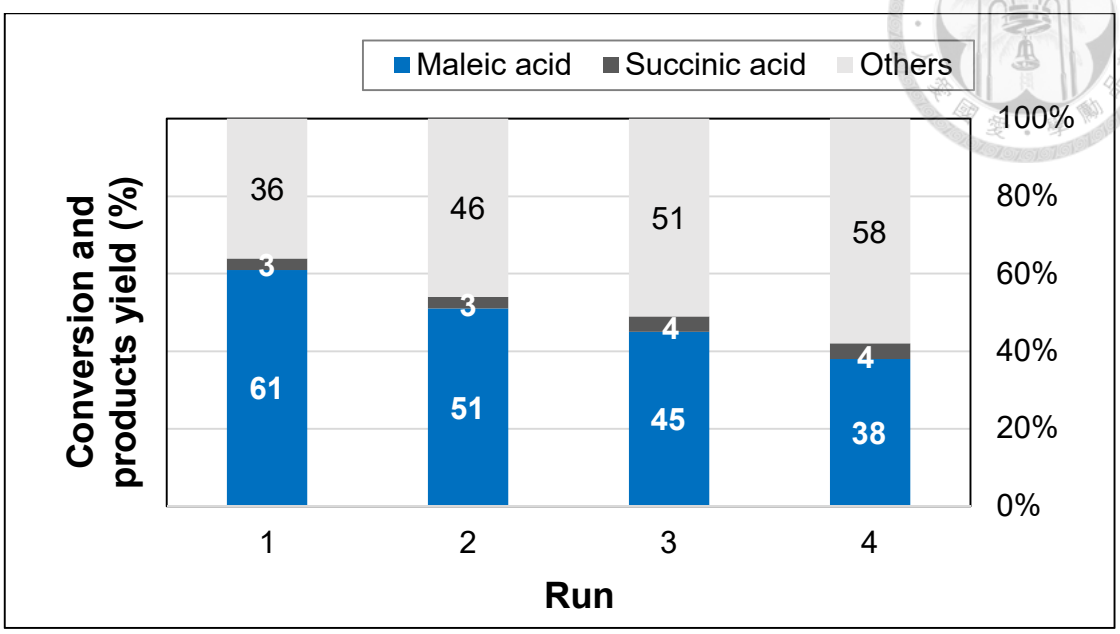

Figure 5.13 Recycle test

(Reaction conditions: Furfural 1 mmol, NC-900 50 mg, H_2O_2 35 wt% 5 mL, H_2O 5 mL, 80 °C, 5 h)

Table 5.3 The composition of the fresh and spent NC-900 materials

Materials	Elemental analysis (wt%)		XPS N 1s (%)			
	N	C	Pyridinic-N (N-6)	Pyrrolic-N (N-5)	Graphitic-N (N-Q)	Oxide-N (N-O)
Fresh NC-900	14.29	63.59	47.56	27.6	24.84	0
Spent NC-900	10.6	48.261	58.4	26.3	12.2	3.1

doi:10.6342/NTU201901225

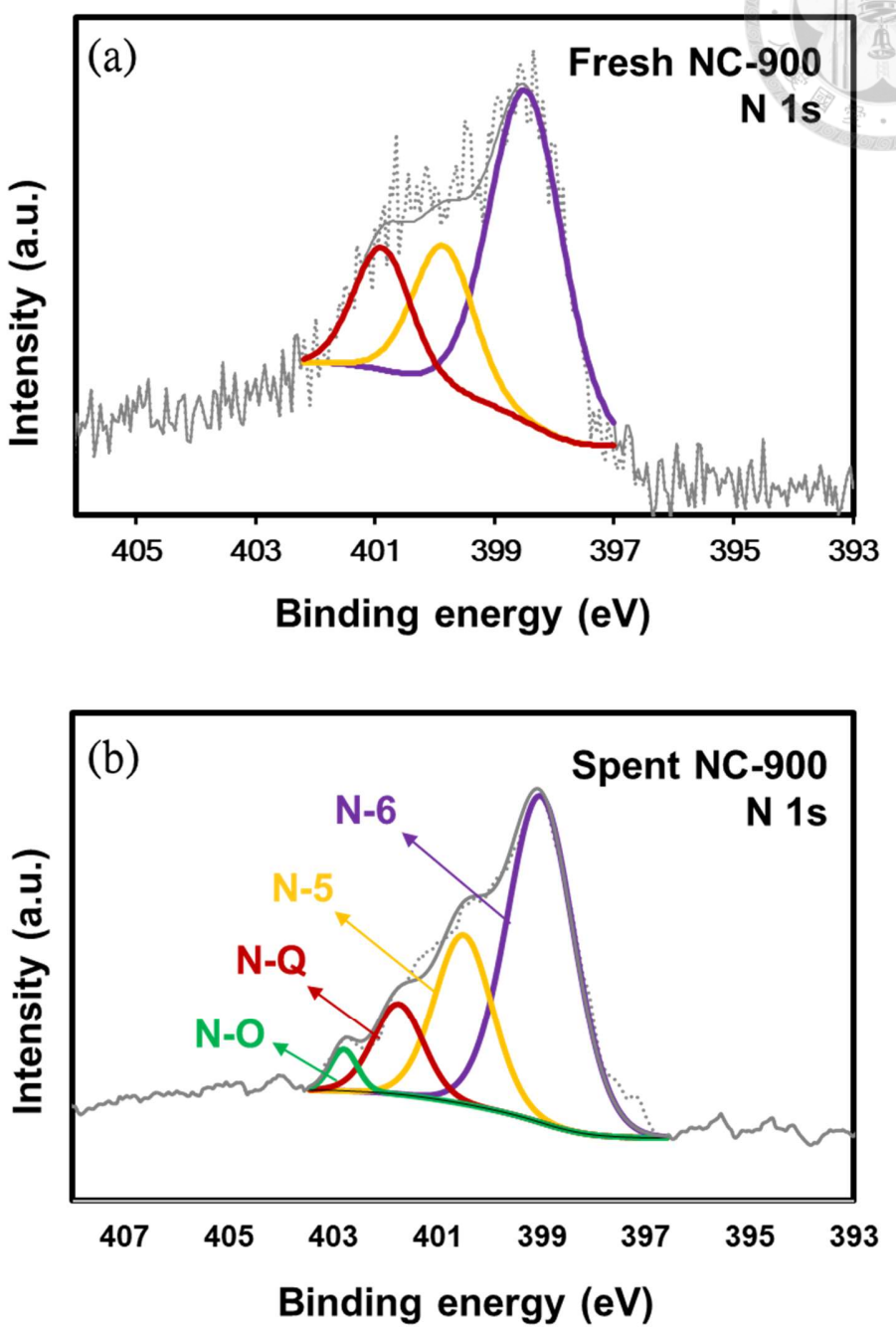

Figure 5.14 XPS pattern of (a) fresh NC-900 and (b) spent NC-900

doi:10.6342/NTU201901225

5.4. Product purification

Typically, after the reaction, the catalyst was separated away from the product mixture by syringe filtration (0.22 μm pore size). Other than the main product (i.e. maleic acid), the product mixture also contained a different kind of carboxylic acids side products such as succinic acid, fumaric acid, 2-furoic acid and formic acid. First, an aqueous NaOH solution (50 wt%) was incorporated to precipitate the carboxylic acids to become carboxylate salts. An important thing is that only an exact amount of NaOH (no. of mol NaOH / MA = 1) was added in order to recover the most acidic proton (first p*K*a) of the MA. The first p*K*a of MA is 1.9, well below that of succinic acid (4.2), fumaric acid (3.03), 2-furoic acid (3.12) and formic acid (3.73), consequently the first proton of MA will first be neutralized. The number of moles of MA was quantified by the calibration curve from HPLC. After rotary evaporate, the sodium maleate salt and the acid side products are all in solid form. Ether which dissolves the acid side products but does not dissolve salt was used to extract the acid side products in order to remove them. Then by centrifugation, ether solvent was removed, to obtain dry sodium maleate salt. Then by adding hydrochloric acid, sodium maleate salt was transformed back to the maleic acid. However, along with this step, the co-product, NaCl also formed. Therefore, an additional step was needed, in which acetone was used to dissolve MA while the NaCl which do not dissolve in acetone will be left. Lastly, by centrifugation, we removed the acetone and dried the final product overnight in vacuum. By this procedure, a maleic acid purity ≥ 98% was obtained on HPLC grade. The HPLC chromatogram before and after the purification process were shown in appendix.

doi:10.6342/NTU201901225

5.5. Reaction mechanism studies

According to the reported literature, there were several possible reaction pathways for the catalytic oxidation of furfural to maleic acid. We are going to interpret each of them, to have understanding on the mechanism that involved in our reaction system.

One possible reaction pathway involved the Baeyer-Villiger oxidation of furfural as the first step to produce furanol formate ester, whom was then hydrolyzed to 2-hydroxyfyuran and formic acid[65,69,76]. At the same time, 2-hydroxyfyuran was in equilibrium with the other two tautomeric isomers: furan-2(3H)-one and furan-2(5H)-one, where the former yields SA and the latter yields MA after the corresponding oxidation steps. The presence of these tautomeric species explained the reason why SA and MA are always formed simultaneously and why the selectivity of SA or MA can be tuned by changing the H_2O_2 / furfural ratio, in which MA requires more H_2O_2 to be formed. Because both formic acid and furan-2(5H)-one were observed in our reaction, thus we considered that the present reaction may proceed through this reaction pathway.

doi:10.6342/NTU201901225

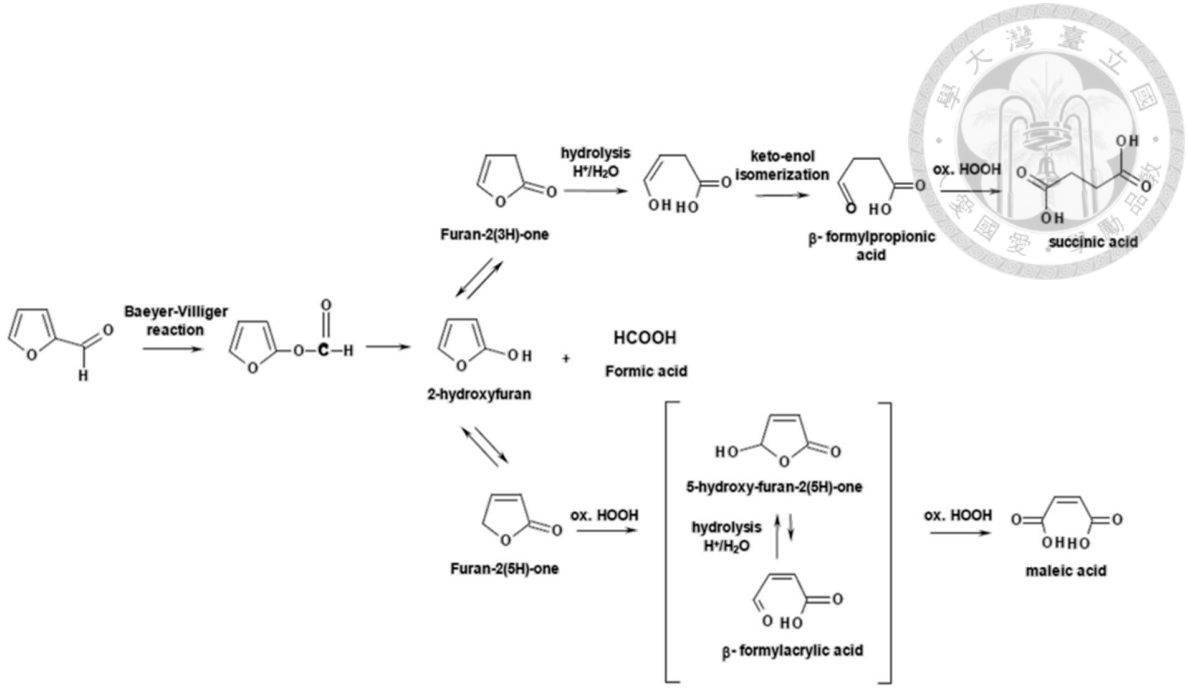

Figure 5.16 The proposed reaction mechanism starts with Baeyer-Villiger oxidation of furfural[69]

On the other hand, Granados et al. had proposed a different mechanism[69] based on the results and the proposal form Jacobs et al. on oxidizing of furan to maleic dialdehyde[77]. Based on Jacobs et al., one of the double bonds in the furan rings was undergoes epoxidation and rearrangement to produce 1,4-dicarbonyl compounds. The same epoxidation and rearrangement steps can be applied to furfural, in which the double bond with less steric hindrance was more selectively to be epoxidized, and the furfural-epoxide will rapidly undergo rearrangement to yield Z-4-oxopent-2-enedial. Thus, Granados's group proposed that the formation of a C_4 intermediate occurs through Baeyer-Villiger oxidation of the aldehyde functionality at 1-position of the Z-4-oxopent-2-enedial. Then, an ester was formed, which rapidly hydrolyzed to form β-formylacrylic acid ((Z)-4-oxobuten-2-enoic acid), along with the releasing of formic acid to form maleic acid.

doi:10.6342/NTU201901225

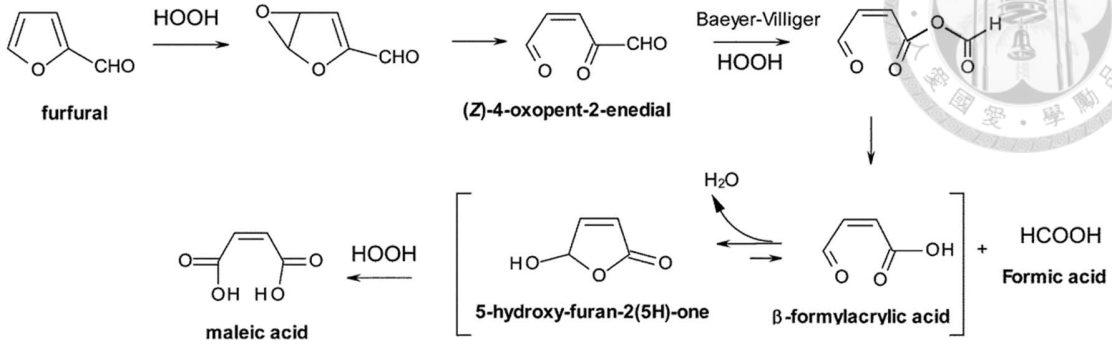

Figure 5.17 The proposed reaction mechanism via epoxidation of the furan ring[68]

Another possible pathway is the 2-furoic acid route[65,69] as shown in Figure 5.18, where the reaction starts with the oxidation of furfural to furoic acid. Subsequently, the furoic acid was transformed to furan by decarboxylation, followed by the further oxidation of furan by H_2O_2 to form MA. However, this possibility can be discarded because when the oxidation of furoic acid with H_2O_2 was conducted by using NC-900 (reactant 1 mmol, NC-900 catalyst 50 mg, 5 mL 35 wt% H_2O_2, 5 mL H_2O, T = 80 °C, time = 5 h.), the MA yield was much lower than that obtained by using furfural as the reactant. Thus, we can ensure that 2-furoic acid is not the intermediate in our reaction, and the 2-furoic acid route was not involved in our reaction system.

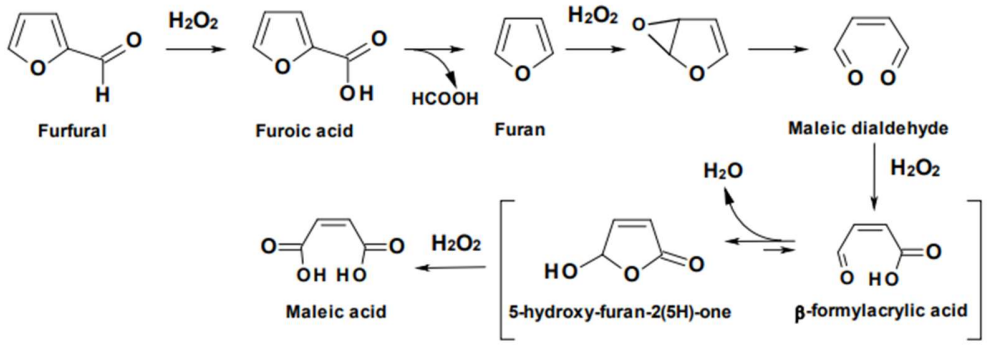

Figure 5.18 The proposed reaction mechanism via epoxidation of furoic acid[68]

doi:10.6342/NTU201901225

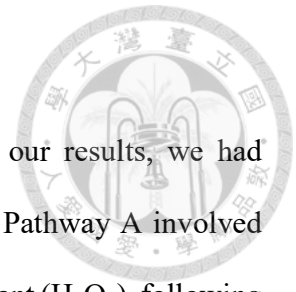

Therefore, according to these reported reaction pathways and our results, we had summed up two possible reaction pathways involved in our reaction. Pathway A involved Baeyer-Villiger oxidation as the first step under the effect of strong oxidant (H_2O_2), following by hydrolysis and rearrangement to form 2(5H)-furanone as the intermediate, producing both maleic acid and succinic acid. On the other hand, in pathway B, furfural undergoes oxidative ring-opening reaction, Baeyer-Villiger oxidation, rearrangement steps, and hydrolysis to form 5-hydroxy-furan-2(5H)-one as the main intermediate. In our reaction system, the selectivity towards 2(5H)-furanone was very low, and its amount was also not corresponded to the MA yield. So, we suggest that our reaction does not proceed through pathway A. In order to confirm this hypothesis, instead of furfural, 2(5H)-furanone was used as the reactant in the similar oxidation reaction. There was only a small amount of SA but no MA yield detected after 5-hours reaction time.

Moreover, the results from the time-dependent analysis showed the decrease of the main intermediate, 5-hydroxy-2(5H)-furanone and the increase of the final product, maleic acid, at the same time. Thus, we proposed that Pathway B is the main reaction pathway that involved in our case, with 5-hydroxy-2(5H)-furanone as the main intermediate, whereas the Pathway A was regarded as an unfavorable pathway which leads to the formation of succinic acid as the side product.

doi:10.6342/NTU201901225

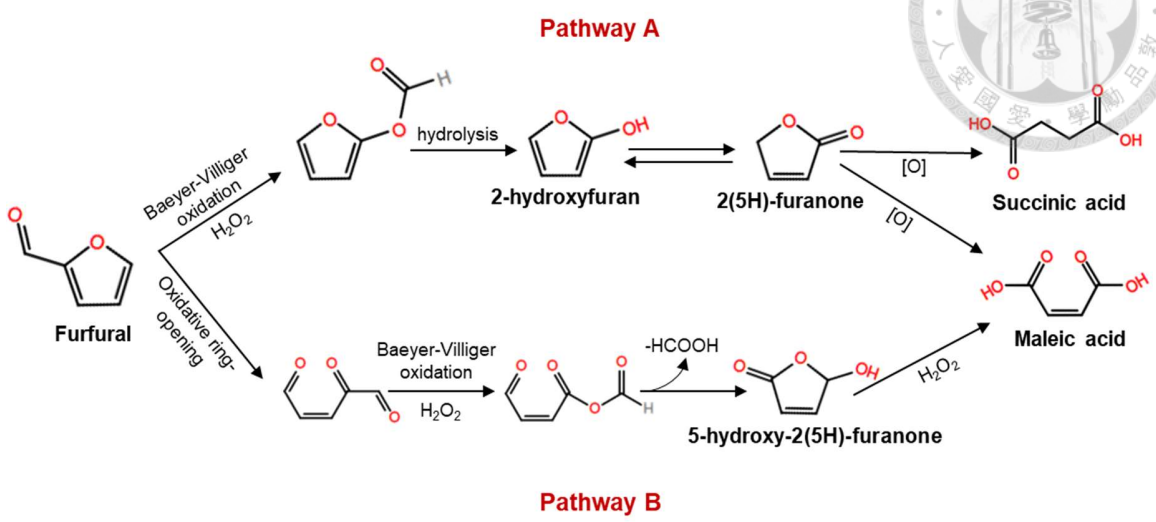

Figure 5.19 The proposed reaction mechanism in the present study

doi:10.6342/NTU201901225

5.6. The effect of different furan substrate

In order to investigate the influence of substrate structure on the current reaction, various furan compounds were tested under the same reaction system with NC-900 as the catalyst. All the furan compounds listed in Table 5.4 can be derived from biomass platform molecules except the unsubstituted furan. Both furfural and HMF can obtain from biomass-derived carbohydrates. 2-furoic acid was obtained from the oxidation of furfural, while 2,5-furandicarboxylic acid (FDCA) can be derived from the oxidation or hydrogenation of HMF. Both furan compounds without functional group and furan substituted with aldehyde group (i.e. furfural and HMF) give a 100% conversion at 80 °C in 5 hours (Table 5.4, entry 1-3). Meanwhile, the furan compounds substituted with carboxylic acid group showed a lower conversion, which ranges from 72 - 84% (Table 5.4, entry 4-5). Furthermore, a variety of MA yield was observed with 41%, 60%, 28%, 38%, and 40% for furan, furfural, 5-hydroxymethylfurfural (HMF), 2-furoic acid, and 2,5-furandicarboxylic acid (FDCA), respectively.

doi:10.6342/NTU201901225

Table 5.4 The oxidation of furan compounds to MA over NC-*x* catalyst

	Reactant	Conversion (%)	Yield (%)		
			Maleic acid	Succinic acid	Others
	Furan 	100	41	0	59
Furan ring substituted with **aldehyde group**	Furfural 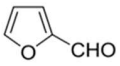	100	61	3	36
	HMF 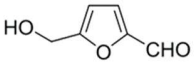	100	28	5	67
Furan ring substituted with **carboxylic acid group**	2-furoic acid 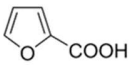	84	38	2	44
	FDCA 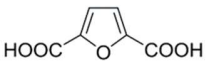	72	40	2	30
Reaction conditions: Reactants (1 mmol), NC-900 catalyst (50 mg), 5 mL H_2O_2 (35 wt%), 5 mL H_2O, T = 80 °C, time = 5 h					

doi:10.6342/NTU201901225

5.7. The effect of different sources-derived NC

Furthermore, we synthesized the nitrogen-doped carbon materials from different sources, such as melamine and biomass, to compare with the ZIF-8 derived N-doped carbon. Graphitic carbon nitride (g-C_3N_4) is a promising material for photocatalytic application owing to its unique electronic and optical properties. It was synthesized by direct heating of the nitrogen-rich precursor, melamine in air[71]. And, the inexpensive, abundant and renewable material, chitosan was used as the precursor for the preparation of nitrogen-doped carbon materials according to the experimental procedure in literature[72]. To further improve the nitrogen content, a nitrogen-enriched raw material, urea, was also added as a co-precursor. The as-prepared biomass-NC material showed high catalytic activity to promote the oxidation of HMF to DFF in the reported study.

The similarity between these two materials with the ZIF-8-derived nitrogen-doped carbon is that all of them exhibited a high nitrogen content, which was further confirmed by the elemental analysis in Table 5.6. Especially for the g-C_3N_4, contained about 60 wt% of Nitrogen. However, when the furfural to maleic acid conversion was carried out by using these catalysts under the same reaction conditions, an extremely low amount of MA yield was obtained. Table 5.5 demonstrated the comparison of the catalytic activity of these catalyst in furfural oxidation reaction. A high furfural conversion (98% - 100%) was achieved by all tested catalyst, but the melamine-derived g-C_3N_4 and biomass-derived NC give an extremely low MA yield, with 20% and 18% in 5 hours, respectively. Compared to these catalysts, the ZIF-8-derived NC showed the highest yield, with 61% of MA at the same reaction conditions.

By XPS, we analyzed the N-C bonds in g-C_3N_4, biomass-derived NC, and ZIF-8-derived NC-900, which were shown in Table 5.6 and Figure 5.20. It can be identified that the

doi:10.6342/NTU201901225

N-Q species contained in g-C_3N_4 and biomass-derived NC catalyst is 1.85% and 4.7% respectively, which is much lower than the amount contained in ZIF-8-derived NC-900. The difference in the N 1s configuration structure of these materials become the key factor that affecting the difference in their catalytic activity. Again, this became an important evidence to confirm the important role of N-Q bond in the catalytic reaction in our system.

Table 5.5 The effect of different sources-derived NC material on furfural oxidation

Sources	Nitrogen-doped carbon material			Conversion (%)	Maleic acid yield (%)
MOF 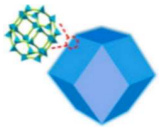	ZIF-8	**900 °C, 8 h, N_2**	NC-900	100	61
Chemical 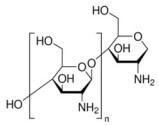	melamine ($C_3H_6N_6$)	**520 °C, 4 h, O_2**	graphitic carbon nitride (g-C_3N_4)	100	20
Biomass 	chitosan + urea	**900 °C, 5 h, N_2**	biomass-derived NC	97	18

doi:10.6342/NTU201901225

Table 5.6 The composition of the NC materials derived from different sources

Materials	Elemental analysis (wt%)		XPS N 1s (%)		
	N	C	Pyridinic-N (N-6)	Pyrrolic-N (N-5)	Graphitic-N (N-Q)
g-C_3N_4	60.81	34.34	80.63	17.52	1.85
biomass-NC	8.52	71.47	55.5	39.8	4.7
NC-900	14.29	63.59	47.56	27.6	24.84

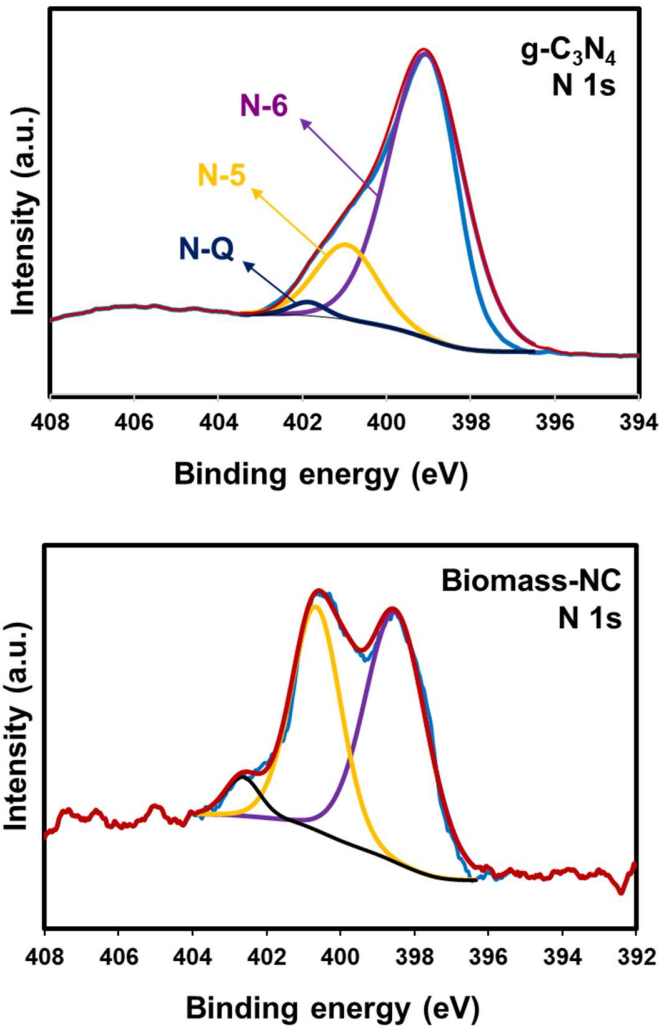

Figure 5.20 XPS pattern of the NCs derived from different sources

doi:10.6342/NTU201901225

6. Conclusions

We have demonstrated the effect of an acid-free carbon material for the conversion of furfural to maleic acid for the first time. The nitrogen-doped carbon catalyst, synthesized from ZIF-8, exhibited a high catalytic activity in the furfural oxidation reaction. Under the optimized reaction conditions (i.e. NC-900 as a catalyst, water as solvent, assisted with 5 mL of 35% H_2O_2 and conducted at 80 °C for 5 hours), 61% yield toward MA was achieved. Our results reveal that the graphitic-N (N-Q) species playing a significant role for the formation of active site which enhanced the catalytic activity. In addition, the NC-900 can be reused for four time but the catalytic activity decrease due to deactivation of the catalyst during recycle test. Maleic acid purity ≥ 98% on HPLC grade was also obtained through the developed purification process. In addition, we compare the catalytic activity of N-doped carbon catalyst synthesized from different sources. The ZIF-8-derived NC exhibits the best catalytic performance for the conversion of furfural to MA, compared to the g-C_3N_4 and biomass-derived NC due to the difference in bonding configurations of nitrogen. Overall, we provide a green synthesis way (i.e. acid-free and metal-free) to convert the biomass-derived platform chemicals into fine chemicals, which might be potential for other organic synthesis process.

doi:10.6342/NTU201901225

7. Future Prospect

Activation energy presents how large is the energy barrier of reaction and provides a better explanation and evidence on kinetic performance of the reaction. Thus, we are interested to know the value of activation energy in our reaction system. However, some difficulty exists, due to the presence of several side products in our case. Therefore, effort will be putting on calculation the value of activation energy and the value of the reaction order in our reaction system.

doi:10.6342/NTU201901225

8. References

1 Kurt Lohbeck , H. H., Werner Fuhrmann, Norbert Fedtke, Maleic and Fumaric Acids, **2000**, 22

2 Felthouse, T. B., J. Mitchell, S. Mummey, Maleic anhydride, Maleic acid, and Fumaric acid, **1997**, 15

3 Delhomme, C., Weuster-Botz, D. & Kühn, F. E., Succinic acid from renewable resources as a C4building-block chemical-a review of the catalytic possibilities in aqueous media, *Green Chem.,* **2009**, 11, 13-26

4 Maleic Anhydride Market - Global Industry Analysis, Size, Share, Growth, Trends and Forecast, 2012 - 2018, *Transparency Market Research (TMR),* **2013**

5 Albonetti, S., Cavani, F. & TrifirÒ, F., Key Aspects of Catalyst Design for the Selective Oxidation of Paraffins, *Catalysis Reviews,* **1996**, 38, 413-438

6 Centi, G., Trifiro, F., Ebner, J. R. & Franchetti, V. M., Mechanistic aspects of maleic anhydride synthesis from C4 hydrocarbons over phosphorus vanadium oxide, *Chemical Reviews,* **1988**, 88, 55-80

7 Alonso, D. M., Bond, J. Q. & Dumesic, J. A., Catalytic conversion of biomass to biofuels, *Green Chemistry,* **2010**, 12, 1493-1513

8 Huber, G. W., Iborra, S. & Corma, A., Synthesis of transportation fuels from biomass: chemistry, catalysts, and engineering, *Chemical reviews,* **2006**, 106, 4044-4098

9 Dutta, S., De, S., Saha, B., Alam, M. I. J. C. S. & Technology, Advances in conversion of hemicellulosic biomass to furfural and upgrading to biofuels, **2012**, 2, 2025-2036

10 Gallezot, P., Conversion of biomass to selected chemical products, *Chemical Society Reviews,* **2012**, 41, 1538-1558

11 Gallezot, P., Catalytic routes from renewables to fine chemicals, *Catalysis Today,* **2007**, 121, 76-91

12 Hu, L. *et al.*, Catalytic conversion of biomass-derived carbohydrates into fuels and chemicals via furanic aldehydes, *Rsc Advances,* **2012**, 2, 11184-11206

13 Karinen, R., Vilonen, K. & Niemelä, M., Biorefining: heterogeneously catalyzed reactions of carbohydrates for the production of furfural and hydroxymethylfurfural, *ChemSusChem,* **2011**, 4, 1002-1016

14 Mamman, A. S. *et al.*, Furfural: Hemicellulose/xylose derived biochemical, *Biofuels, Bioproducts and Biorefining,* **2008**, 2, 438-454

15 Brownlee Harold J, M. C. S., Industrial Development of Furfural, *Industrial Engineering Chemistry,* **1948**, 40, 201-204

16 Bozell, J. J. & Petersen, G. R., Technology development for the production of biobased products from biorefinery carbohydrates - the US Department of Energy's "Top 10" revisited, *Green Chemistry,* **2010**, 12, 539-554

doi:10.6342/NTU201901225

17 Chheda, J. N. & Dumesic, J. A., An overview of dehydration, aldol-condensation and hydrogenation processes for production of liquid alkanes from biomass-derived carbohydrates, *Catalysis Today,* **2007**, 123, 59-70
18 Huber, G. W., Chheda, J. N., Barrett, C. J. & Dumesic, J. A., Production of liquid alkanes by aqueous-phase processing of biomass-derived carbohydrates, *Science,* **2005**, 308, 1446-1450
19 Li, X., Jia, P. & Wang, T., Furfural: A promising platform compound for sustainable production of C4 and C5 chemicals, *ACS Catalysis,* **2016**, 6, 7621-7640
20 Zhang, J., Zhao, Z., Xia, Z. & Dai, L., A metal-free bifunctional electrocatalyst for oxygen reduction and oxygen evolution reactions, *Nature nanotechnology,* **2015**, 10, 444
21 Zheng, Y. *et al.*, Hydrogen evolution by a metal-free electrocatalyst, *Nature communications,* **2014**, 5, 3783
22 Yang, L. *et al.*, Boron-doped carbon nanotubes as metal-free electrocatalysts for the oxygen reduction reaction, *Angewandte Chemie International Edition,* **2011**, 50, 7132-7135
23 Hu, C. & Dai, L., Carbon-based metal-free catalysts for electrocatalysis beyond the ORR, *Angewandte Chemie International Edition,* **2016**, 55, 11736-11758
24 Liu, X. & Dai, L., Carbon-based metal-free catalysts, *Nature Reviews Materials,* **2016**, 1, 16064
25 Shui, J., Wang, M., Du, F. & Dai, L., N-doped carbon nanomaterials are durable catalysts for oxygen reduction reaction in acidic fuel cells, *Science advances,* **2015**, 1, 1400129
26 Wei, Q. *et al.*, Nitrogen-doped carbon nanotube and graphene materials for oxygen reduction reactions, *Catalysts,* **2015**, 5, 1574-1602
27 Zhao, Y. *et al.*, Can boron and nitrogen co-doping improve oxygen reduction reaction activity of carbon nanotubes?, *Journal of the American Chemical Society,* **2013**, 135, 1201-1204
28 Zhao, Y., Nakamura, R., Kamiya, K., Nakanishi, S. & Hashimoto, K., Nitrogen-doped carbon nanomaterials as non-metal electrocatalysts for water oxidation, *Nature communications,* **2013**, 4, 2390
29 Kumar, B. *et al.*, Renewable and metal-free carbon nanofibre catalysts for carbon dioxide reduction, *Nature communications,* **2013**, 4, 2819
30 Chaikittisilp, W., Ariga, K. & Yamauchi, Y., A new family of carbon materials: synthesis of MOF-derived nanoporous carbons and their promising applications, *Journal of Materials Chemistry A,* **2013**, 1, 14-19
31 Wood, K. N., O'Hayre, R. & Pylypenko, S., Recent progress on nitrogen/carbon structures designed for use in energy and sustainability applications, *Energy Environ. Sci.,* **2014**, 7, 1212-1249

doi:10.6342/NTU201901225

32 Deng, Y., Xie, Y., Zou, K. & Ji, X., Review on recent advances in nitrogen-doped carbons: preparations and applications in supercapacitors, *Journal of Materials Chemistry A,* **2016**, 4, 1144-1173
33 Furukawa, H., Cordova, K. E., O'Keeffe, M. & Yaghi, O. M., The chemistry and applications of metal-organic frameworks, *Science,* **2013**, 341, 1230444
34 Perez, E., Karunaweera, C., Musselman, I., Balkus, K. & Ferraris, J., Origins and Evolution of Inorganic-Based and MOF-Based Mixed-Matrix Membranes for Gas Separations, *Processes,* **2016**, 4, 32
35 Kaye, S. S., Dailly, A., Yaghi, O. M. , Long, J. R., Impact of preparation and handling on the hydrogen storage properties of Zn4O(1,4-benzenedicarboxylate)(3) (MOF-5), *Journal of the American Chemical Society,* **2007**, 129, 14176
36 Li, J.-R., Kuppler, R. J. & Zhou, H.-C., Selective gas adsorption and separation in metal–organic frameworks, *Chemical Society Reviews,* **2009**, 38, 1477-1504
37 An, J., Geib, S. J. & Rosi, N. L., Cation-triggered drug release from a porous zinc− adeninate metal− organic framework, *J. Am. Chem. Soc.,* **2009**, 131, 8376-8377
38 Hu, Z., Deibert, B. J. & Li, J., Luminescent metal–organic frameworks for chemical sensing and explosive detection, *Chemical Society Reviews,* **2014**, 43, 5815-5840
39 Lee, J. *et al.*, Metal-organic framework materials as catalysts, *Chem Soc Rev,* **2009**, 38, 1450-1459
40 Zhu, Q. L. & Xu, Q., Metal-organic framework composites, *Chem Soc Rev,* **2014**, 43, 5468-5512
41 Liu, B., Shioyama, H., Akita, T. & Xu, Q., Metal-organic framework as a template for porous carbon synthesis, *Journal of the American Chemical Society,* **2008**, 130, 5390-5391
42 Huang, G. *et al.*, Metal-Organic Framework-Templated Porous Carbon for Highly Efficient Catalysis: The Critical Role of Pyrrolic Nitrogen Species, *Chemistry,* **2016**, 22, 3470-3477
43 Xia, W., Mahmood, A., Zou, R. & Xu, Q., Metal–organic frameworks and their derived nanostructures for electrochemical energy storage and conversion, *Energy & Environmental Science,* **2015**, 8, 1837-1866
44 Hayashi, H., Cote, A. P., Furukawa, H., O'Keeffe, M. & Yaghi, O. M., Zeolite A imidazolate frameworks, *Nature materials,* **2007**, 6, 501
45 Banerjee, R. *et al.*, High-throughput synthesis of zeolitic imidazolate frameworks and application to CO2 capture, *Science,* **2008**, 319, 939-943
46 Park, K. S. *et al.*, Exceptional chemical and thermal stability of zeolitic imidazolate frameworks, *Proceedings of the National Academy of Sciences,* **2006**, 103, 10186-10191
47 Lee, Y.-R. *et al.*, ZIF-8: A comparison of synthesis methods, *Chemical Engineering Journal,* **2015**, 271, 276-280

doi:10.6342/NTU201901225

48 Pan, Y., Liu, Y., Zeng, G., Zhao, L. & Lai, Z., Rapid synthesis of zeolitic imidazolate framework-8 (ZIF-8) nanocrystals in an aqueous system, *Chemical Communications,* **2011**, 47, 2071-2073

49 Liu, N. L. *et al.*, ZIF-8 Derived, Nitrogen-Doped Porous Electrodes of Carbon Polyhedron Particles for High-Performance Electrosorption of Salt Ions, *Scientific Reports,* **2016**, 6, 28847

50 Ma, W., Du, Y., Wang, N. & Miao, P., ZIF-8 derived nitrogen-doped porous carbon as metal-free catalyst of peroxymonosulfate activation, *Environ Sci Pollut Res Int,* **2017**, 24, 16276-16288

51 Zhong, S., Zhan, C. & Cao, D., Zeolitic imidazolate framework-derived nitrogen-doped porous carbons as high performance supercapacitor electrode materials, *Carbon,* **2015**, 85, 51-59

52 Young, C. *et al.*, Zeolitic imidazolate framework (ZIF-8) derived nanoporous carbon: the effect of carbonization temperature on the supercapacitor performance in an aqueous electrolyte, *Phys Chem Chem Phys,* **2016**, 18, 29308-29315

53 Chao, S. *et al.*, Nitrogen-doped Carbon Derived from ZIF-8 as a High-performance Metal-free Catalyst for Acetylene Hydrochlorination, *Sci Rep,* **2017**, 7, 39789

54 Nguyen, C. V. *et al.*, A metal-free, high nitrogen-doped nanoporous graphitic carbon catalyst for an effective aerobic HMF-to-FDCA conversion, *Green Chemistry,* **2016**, 18, 5957-5961

55 Zhang, L. *et al.*, Highly graphitized nitrogen-doped porous carbon nanopolyhedra derived from ZIF-8 nanocrystals as efficient electrocatalysts for oxygen reduction reactions, *Nanoscale,* **2014**, 6, 6590-6602

56 Zheng, F., Yang, Y. & Chen, Q., High lithium anodic performance of highly nitrogen-doped porous carbon prepared from a metal-organic framework, *Nature communications,* **2014**, 5, 5261

57 Salunkhe, R. R. *et al.*, Fabrication of symmetric supercapacitors based on MOF-derived nanoporous carbons, *J. Mater. Chem. A,* **2014**, 2, 19848-19854

58 Guo, D. *et al.*, Active sites of nitrogen-doped carbon materials for oxygen reduction reaction clarified using model catalysts, *Science,* **2016**, 351, 361-365

59 Faisal, S. N. *et al.*, Pyridinic and graphitic nitrogen-rich graphene for high-performance supercapacitors and metal-free bifunctional electrocatalysts for ORR and OER, *RSC Advances,* **2017**, 7, 17950-17958

60 Wu, J. *et al.*, Nitrogen-doped graphene with pyridinic dominance as a highly active and stable electrocatalyst for oxygen reduction, *ACS applied materials & interfaces,* **2015**, 7, 14763-14769

61 Xing, T. *et al.*, Observation of active sites for oxygen reduction reaction on nitrogen-doped multilayer graphene, *Acs Nano,* **2014**, 8, 6856-6862

62 Watanabe, H., Asano, S., Fujita, S.-i., Yoshida, H. & Arai, M., Nitrogen-Doped, Metal-Free Activated Carbon Catalysts for Aerobic Oxidation of Alcohols, *ACS Catalysis,* **2015**, 5, 2886-2894

doi:10.6342/NTU201901225

63 Long, J. *et al.*, Nitrogen-Doped Graphene Nanosheets as Metal-Free Catalysts for Aerobic Selective Oxidation of Benzylic Alcohols, *ACS Catalysis,* **2012**, 2, 622-631

64 Huan, T. N., Van Khai, T., Kang, Y., Shim, K. B. & Chung, H., Enhancement of quaternary nitrogen doping of graphene oxide via chemical reduction prior to thermal annealing and an investigation of its electrochemical properties, *Journal of Materials Chemistry,* **2012**, 22, 14756

65 Guo, H. & Yin, G., Catalytic Aerobic Oxidation of Renewable Furfural with Phosphomolybdic Acid Catalyst: an Alternative Route to Maleic Acid, *The Journal of Physical Chemistry C,* **2011**, 115, 17516-17522

66 Shi, S., Guo, H. & Yin, G., Synthesis of maleic acid from renewable resources: Catalytic oxidation of furfural in liquid media with dioxygen, *Catalysis Communications,* **2011**, 12, 731-733

67 Araji, N. *et al.*, Synthesis of maleic and fumaric acids from furfural in the presence of betaine hydrochloride and hydrogen peroxide, *Green Chemistry,* **2017**, 19, 98-101

68 Li, X., Ho, B., Lim, D. S. W. & Zhang, Y., Highly efficient formic acid-mediated oxidation of renewable furfural to maleic acid with H_2O_2, *Green Chemistry,* **2017**, 19, 914-918

69 Alonso-Fagúndez, N. *et al.*, Aqueous-phase catalytic oxidation of furfural with H_2O_2: high yield of maleic acid by using titanium silicalite-1, *Rsc Advances,* **2014**, 4, 54960-54972

70 Alonso, D. M., Wettstein, S. G. & Dumesic, J. A., Gamma-valerolactone, a sustainable platform molecule derived from lignocellulosic biomass, *Green Chemistry,* **2013**, 15, 584

71 Pawar, R. C. *et al.*, Room-temperature synthesis of nanoporous 1D microrods of graphitic carbon nitride (g-C_3N_4) with highly enhanced photocatalytic activity and stability, *Sci Rep,* **2016**, 6, 31147

72 Ren, Y. *et al.*, Selective and metal-free oxidation of biomass-derived 5-hydroxymethylfurfural to 2,5-diformylfuran over nitrogen-doped carbon materials, *Green Chemistry,* **2018**, 20, 4946-4956

73 Gao, Y. *et al.*, Nitrogen-doped sp^2-hybridized carbon as a superior catalyst for selective oxidation, *Angew Chem Int Ed Engl,* **2013**, 52, 2109-2113

74 Shao, Y. *et al.*, Nitrogen-doped graphene and its electrochemical applications, *Journal of Materials Chemistry,* **2010**, 20, 7491-7496

75 Sroka, Z. & Cisowski, W., Hydrogen peroxide scavenging, antioxidant and anti-radical activity of some phenolic acids, *Food and Chemical Toxicology,* **2003**, 41, 753-758

76 Li, X., Lan, X. & Wang, T., Selective oxidation of furfural in a bi-phasic system with homogeneous acid catalyst, *Catalysis Today,* **2016**, 276, 97-104

77 Wahlen, J. *et al.*, Titanium Silicalite 1 (TS-1) Catalyzed Oxidative Transformations of Furan Derivatives with Hydrogen Peroxide, **2004**, 346, 333-338

doi:10.6342/NTU201901225

Appendix

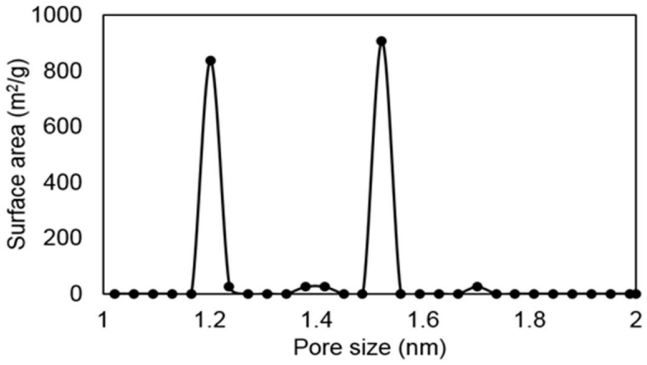

Figure A.1 Pore size distribution of the synthesized ZIF-8 particles

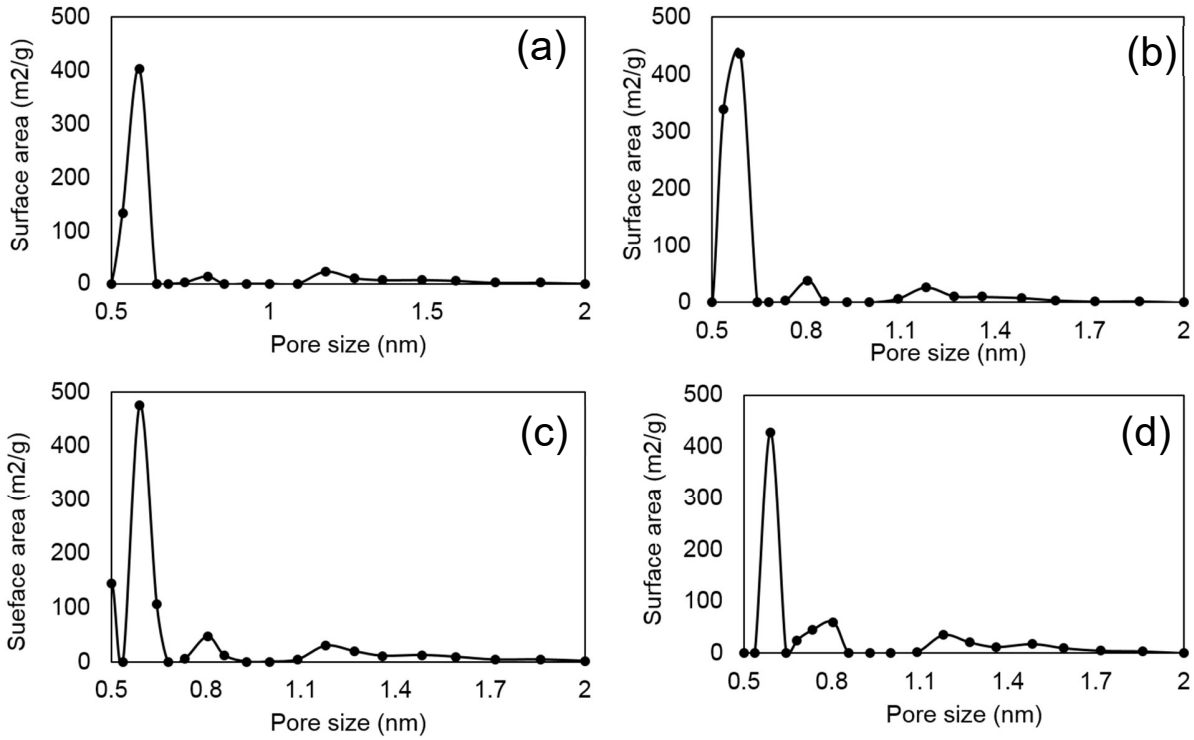

Figure A.2 Pore size distribution of the synthesized NC-*x*

(a) NC-600 (b) NC-700 (c) NC-800 (d) NC-900

doi:10.6342/NTU201901225

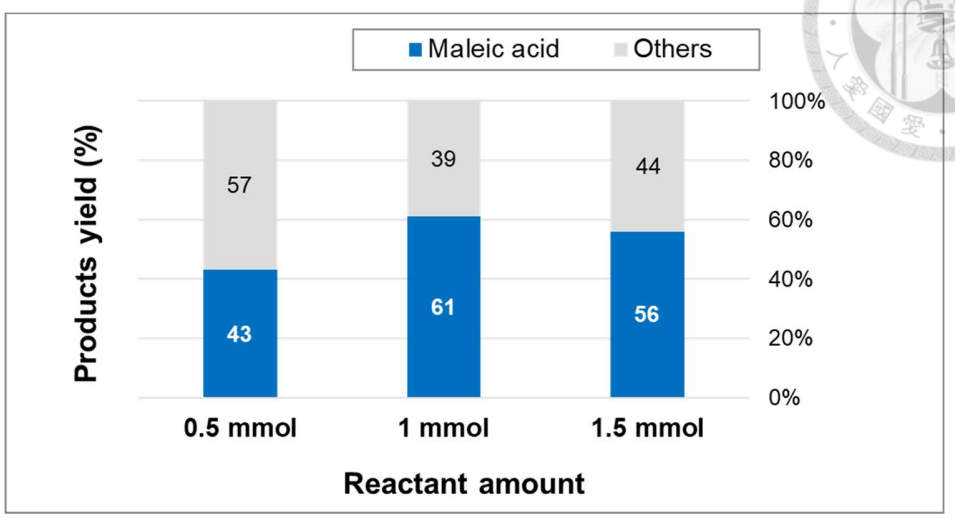

Figure A.3 The effect of reactant amount on furfural to maleic acid reaction

(Reaction conditions: Reactant = furfural, NC-900 50 mg, H_2O_2 35 wt% 5 mL, H_2O 5 mL, 80 °C, 5 h)

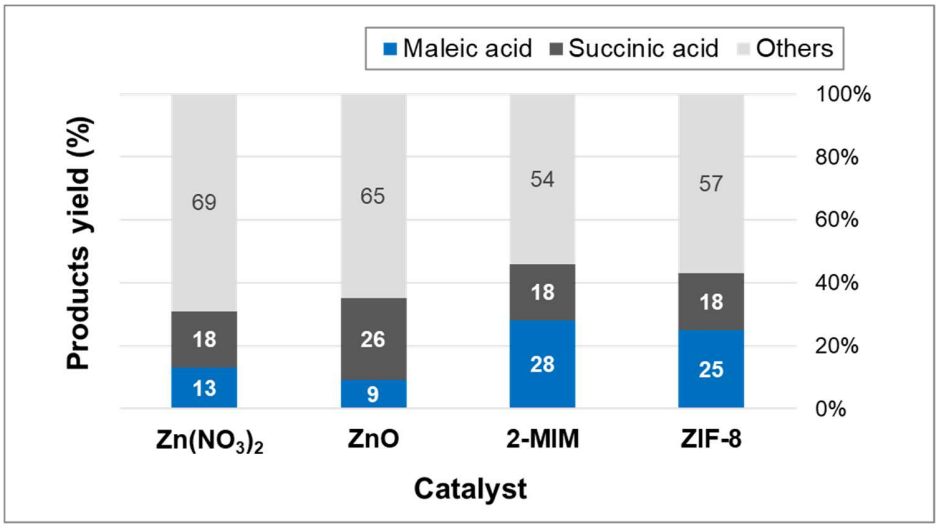

Figure A.4 The effect of catalyst (ZIF-8 precursors) on furfural to maleic acid reaction

(Reaction conditions: Furfural 1 mmol, catalyst 50 mg, H_2O_2 35 wt% 5 mL, H_2O 5 mL, 80 °C, 5 h)

doi:10.6342/NTU201901225

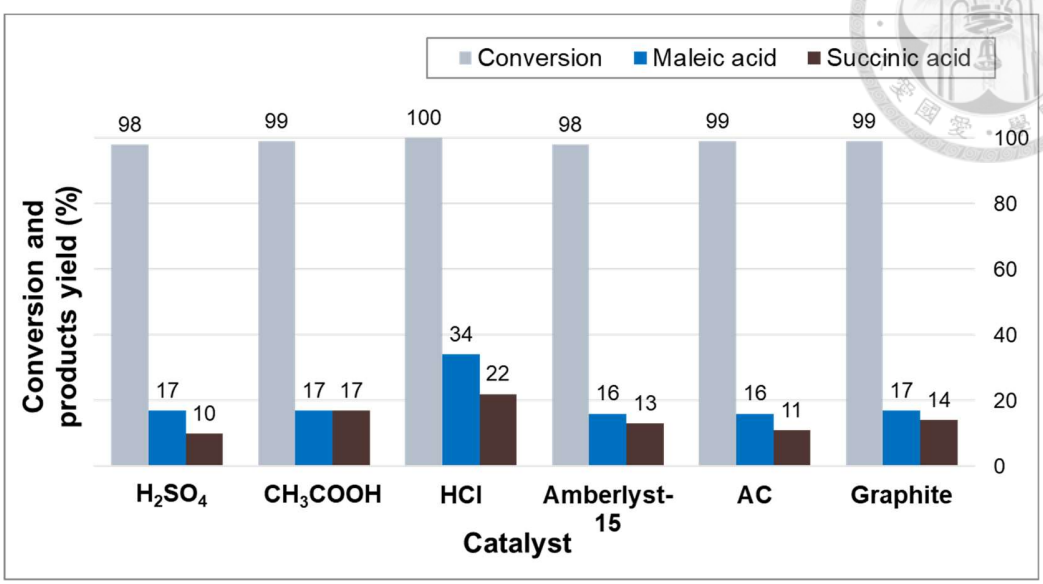

Figure A.5 The effect of catalyst (acidic catalyst & carbon) on furfural to maleic acid reaction (Reaction conditions: Furfural 1 mmol, catalyst 50 mg, H_2O_2 35 wt% 5 mL, H_2O 5 mL, 80 °C, 5 h)

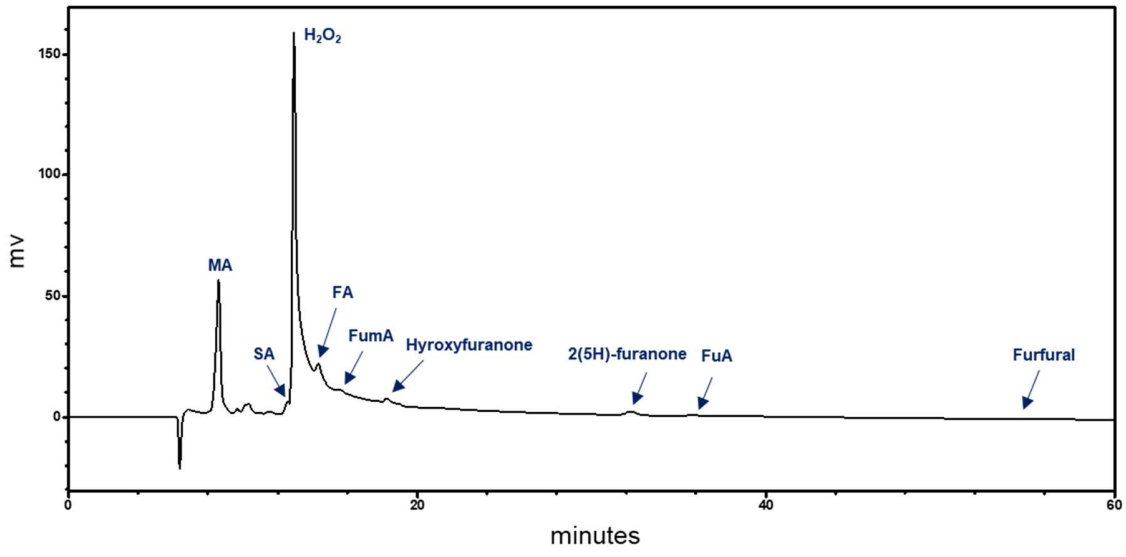

Figure A.6 Typical HPLC chromatogram for furfural to maleic acid reaction

doi:10.6342/NTU201901225

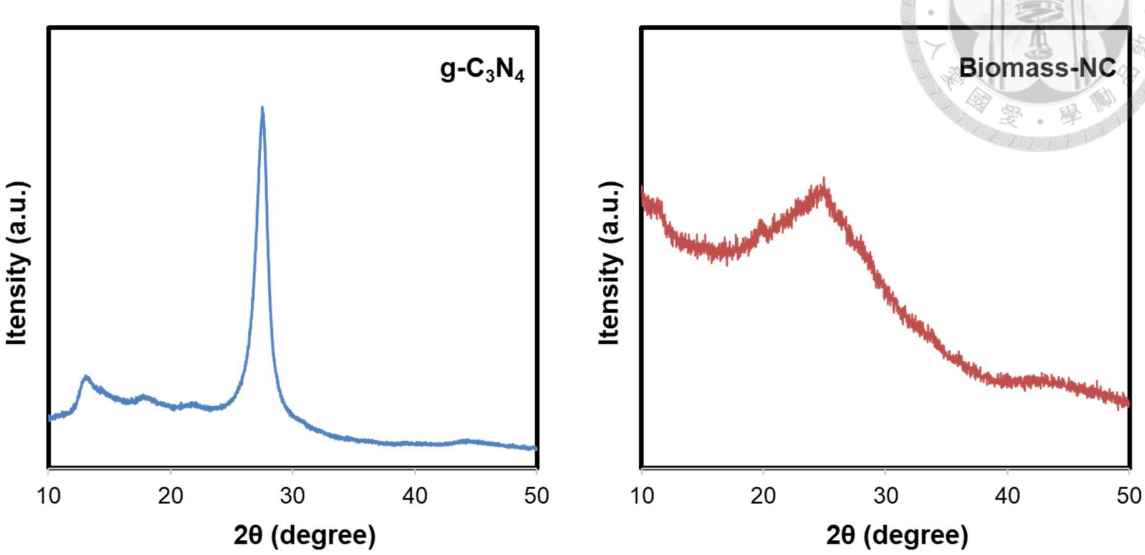

Figure A.7 XRD pattern of g-C_3N_4 and biomass-deirved NC

doi:10.6342/NTU201901225

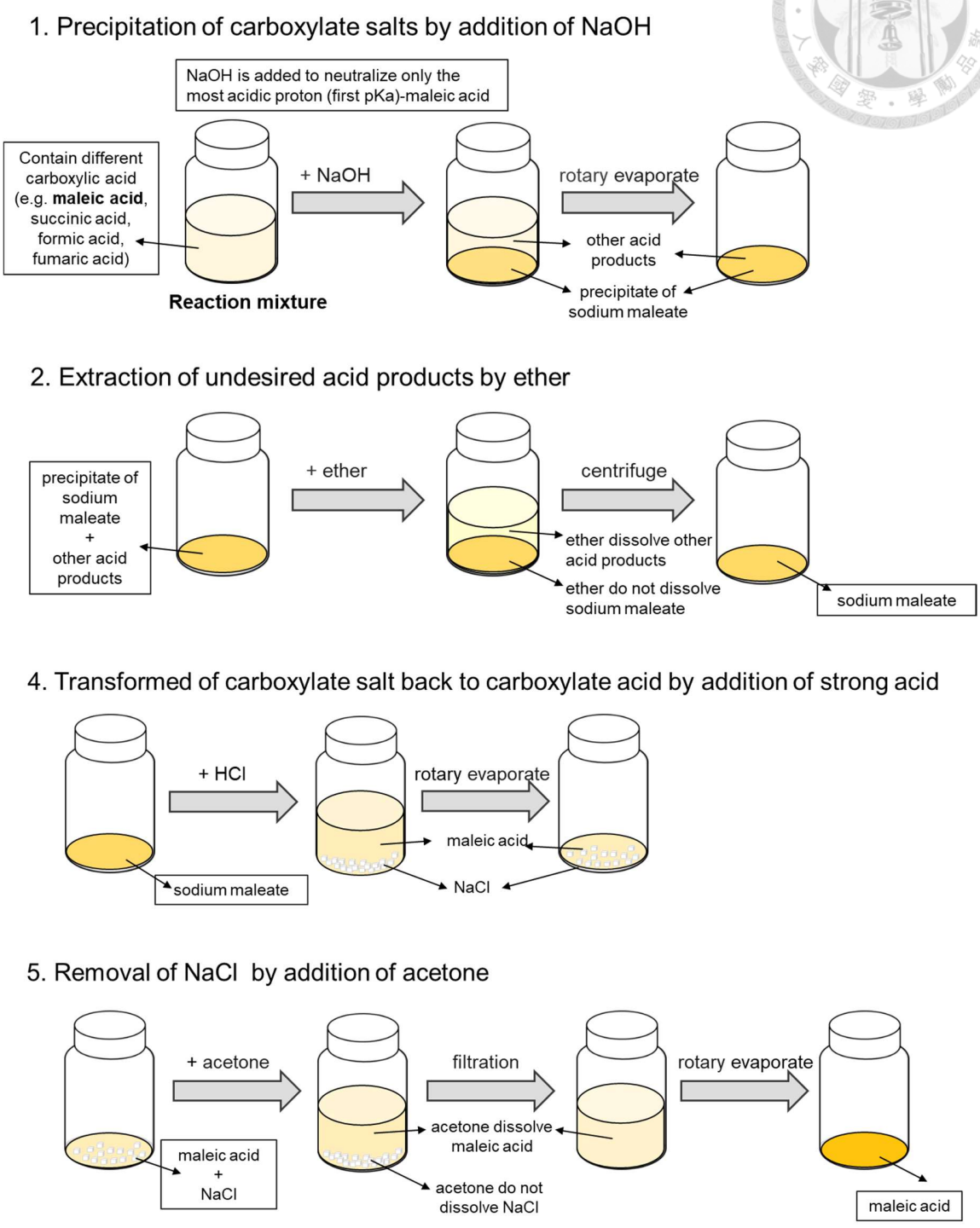

Figure A.8 Detail schematic diagram for product purification process

doi:10.6342/NTU201901225

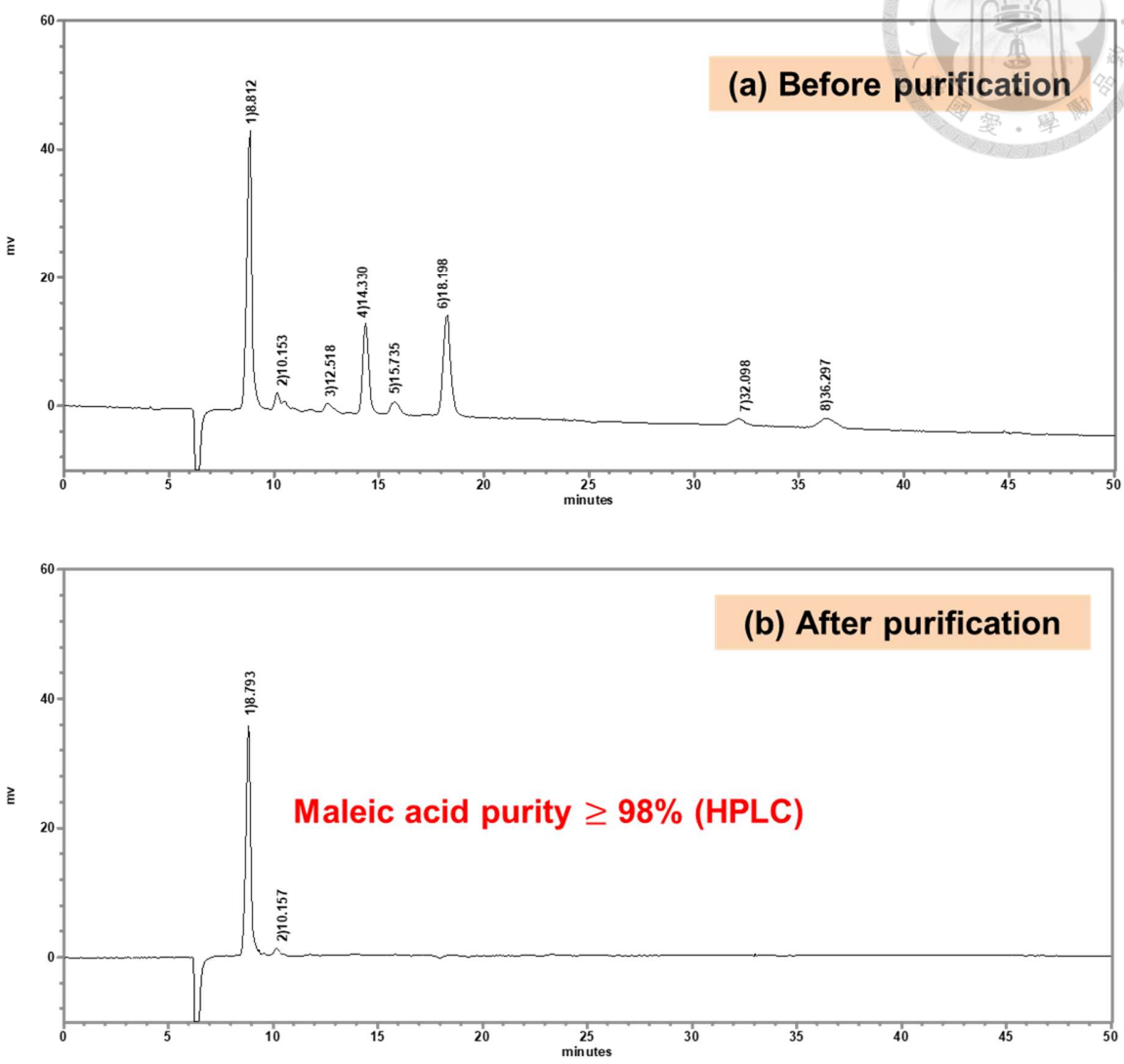

Figure A.9 Typical HPLC chromatogram before and after purification process

doi:10.6342/NTU201901225